Sigma J Eng Nat Sci, Vol. 43, No. 2, pp. 463–486, April, 2025

Sigma Journal of Engineering and Natural Sciences
Web page info: https://sigma.yildiz.edu.tr
DOI: 10.14744/sigma.2025.00036

Research Article

# Numerical and experimental investigation of cross cut angle impact on heat transfer in microchannels

**Vikram M. GHULE[1], Abhay A. PAWAR[1], Lalit N. PATIL[2,*], Vijaykumar K. JAVANJAL[3]**

*[1]Rajarshi Shahu College of Engineering,Tathawade, Pune, 411033, India*
*[2]Department of Automation and Robotics, Dr. D. Y. Patil Institute of Technology, Pimpri, Pune, 411018, India*
*[3]Department of Mechanical Engineering, Dr. D. Y. Patil Institute of Technology, Pimpri, Pune, 411018, India*

## ARTICLE INFO

*Article history*
Received: 10 January 2024
Revised: 15 February 2024
Accepted: 15 March 2024

**Keywords:**
Computational Fluid Dynamics; Heat Transfer; Microchannels; Nanofluids

## ABSTRACT

The present study aims to evaluate experimental investigations of heat transfer and fluid flow performance in cross-cut wavy microchannels with and without nanofluid. It provides a thorough analysis, supported by both numerical simulations and experimental validations, into the impact of cross-cut angles on heat transfer rates in microchannels. A heat flow of 20,000 W/m² was applied to a variety of geometries with cross-cut angles of 0°, 10°, 20°, 30°, 40°, and 50° in computational fluid dynamics (CFD) simulations. Furthermore, experiments using a hydraulic diameter of one millimeter and a Reynolds number range of 100–1000 were conducted to evaluate the viability of the experiments. Increased Reynolds numbers increase Nusselt numbers across geometries by thinning boundary layers. Geometries with cross cuts outperform flat forms due to boundary layer rebuilding and secondary flow. In particular, the geometry with a 30° cross cut exhibits a 41% greater heat transfer rate in testing as compared to its non-cut experimentally. It is observed that geometry of cross cut angle 300 showing maximum Nusselt number 11.497 which is 3.66% greater than that of plain geometry.

**Cite this article as:** Ghule VM, Pawar AA, Patil LN, Javanjal VK. Numerical and experimental investigation of cross cut angle impact on heat transfer in microchannels. Sigma J Eng Nat Sci 2025;43(2):463–486.

## INTRODUCTION

Microelectronic components like transistors, capacitors, inductors, transformers, and resistors serve as the foundational elements in all electronic devices [1]. Any electrical component that experiences current flow must always dissipate heat. Therefore, a rise in heat in electronic circuitry primarily impacts component safety and operating dependability. One of the most significant uses of microchannel technology is the elimination of excessive heat flow from microelectronic circuits [2]. Air serves as the primary coolant in most modern electronic cooling systems. The benefits of air include its extensive development history and experience, minimal auxiliary system support needs, high cooling system dependability, low starting cost, low operating and maintenance costs, and strong compatibility with the microelectronic circuit environment [3].

***Corresponding author.**
*E-mail address: lnpatil_p18@me.vjti.ac.in.com

*This paper was recommended for publication in revised form by Editor-in-Chief Ahmet Selim Dalkilic*

However, the primary issue with air cooling systems is their limited capacity to dissipate heat due to the low specific heat value of air. Heat spreaders are required to enhance the heat transfer surface area due to the low heat transfer coefficient of air cooling [4]. The air-cooled heat sink encounters three elements of thermal resistance with the spreader [5]. These are the spreader's thermal resistance, the spreader's thermal resistance resulting from convection between the fin and the air, including the bonding material's thermal resistance that binds the spreader with the electronic chip [6]. Using a spreader made of high-quality conducting material will lower the spreader resistance. Newton's law of cooling which governs Convective heat transfer from a surface is given in equation 1.

$$Q = hA\ (Ts - Ta) \quad (1)$$

Since the temperature limitations are often set, raising the product hA will increase the heat transfer rate [7]. Microchannels are channels with typical sizes between 10 and 1000 millimeters [8]. Therefore, the surface area for heat transmission is increased by a deep, narrow microchannel that is etched at the backside of a silicon substrate. Due to the lower characteristic dimensions involved, the flow in the microchannel is typically laminar in nature. The Nusselt number (Nu), for an internal flow that is completely developed, is constant [9]. Equation (1.2) provides the Nusselt number.

$$Nu = hD/k \quad (2)$$

Because of their reduced diameter values, the microchannels have the benefit of having very high h values (on the order of several thousand W/m$^2$ °C) [10]. Therefore, in a microchannel, there is a greater convective heat transfer due to the high product hA [11]. Because of this, microchannels are a good solution for high heat removal, with values up to 100 W/cm$^2$.

The majority of researches used theoretical, experimental, and numerical methods to study the performance of rectangular straight microchannel heat sinks [10], [12], [13], [14], [15]. These studies show that microchannel heat sinks can operate more effectively than traditional heat sinks. However, several studies use circular channels in place of rectangular ones to provide a greater cooling effect. Straight channels that are rhombic [13], trapezoidal [16], converging and diverging [17], and transversal [18], [19]. Straight channels are often used in microchannel heat sinks, which results in extremely poor fluid mixing. According to research, nanoparticles improve the thermo-physical characteristics of fluids by increasing diffusivity and conductivity. Zigzag channels exhibit superior heat transfer but with increased pressure drop. The thermal performance of oblique fin microchannels is enhanced by secondary flow and boundary layer rebuilding. Using nanofluids, researchers investigate the effect of oblique fins on cooling in computer server microchannel heat sinks by concentrating on straight channels[20]. Understanding the impact of cross-cut angles on heat transport in microchannels is the driving force for this study [3], [21]. The effectiveness of gas-solid fluidization (GSF) in mass, heat, and mixing transfers makes it a popular process in chemical, petrochemical, and pharmaceutical sectors. Gas flows over a densely packed bed of solid particles in GSF, causing the particles to behave like a fluid with properties that set them apart from both the solid and gas phases. Optimizing industrial processes and guaranteeing their dependable operation need a thorough analysis of GSF systems. Studying the fluidized bed's mass transport, heat transfer, and hydrodynamic properties is a key component of GSF analysis.

The behavior of various pertinent parameters on the fluid flow characteristics is illustrated by some researchers. The qualitative behaviors of velocity, temperature, skin friction, and heat transfer rates of a micropolar fluid are found to be similar for Biot number and radiation parameters. The suction/injection and activation energy parameters increase the concentration of the micropolar fluid within the boundary layer, while the chemical reaction parameter reduces the concentration in the same region. Furthermore, this quadratic convection demonstrates a strong influence on the fluid flow characteristics, with the impact of pertinent parameters being more prominent on the physical quantities compared to the results of linear convection [22], [23]. Through a combination of realistic experiments and numerical simulations, this work attempts to unravel the complex dynamics behind heat dissipation. By improving the design and efficiency of microchannel systems and contributing to the evolution of thermal management technologies for a variety of applications, including industrial heat exchangers and cooling systems for electronics, an understanding of how these cross-cut angles effect heat transmission is possible. This study might lead to the discovery of novel approaches for maximizing heat transmission in microchannels, which would enhance the overall efficiency and performance of these structures. Therefore, it was intended to conduct the numerical and experimental investigation of cross cut angle impact on heat transfer in microchannels.

## MATERIALS AND METHODS

The experimental configuration used for the present research study is displayed in Fig 1. Its primary reservoir is a magnetic stirrer that continually stirs a nano fluid (copper oxide or silver nanowire). A pulsating pump is used to convey the pulsing flow of nano fluid into the microchannel. A differential pressure sensor will be used to monitor the pressure decrease across the microchannel. By monitoring the temperature across the microchannel, including the wall, fluid intake, and exit temperatures, the thermal performance of the microchannel may be ascertained. The microchannel fluid's heat is removed via the condenser unit and second reservoir. With the use of a flow meter, the system's fluid flow rate is determined, and the cooled fluid is then returned to the main reservoir.

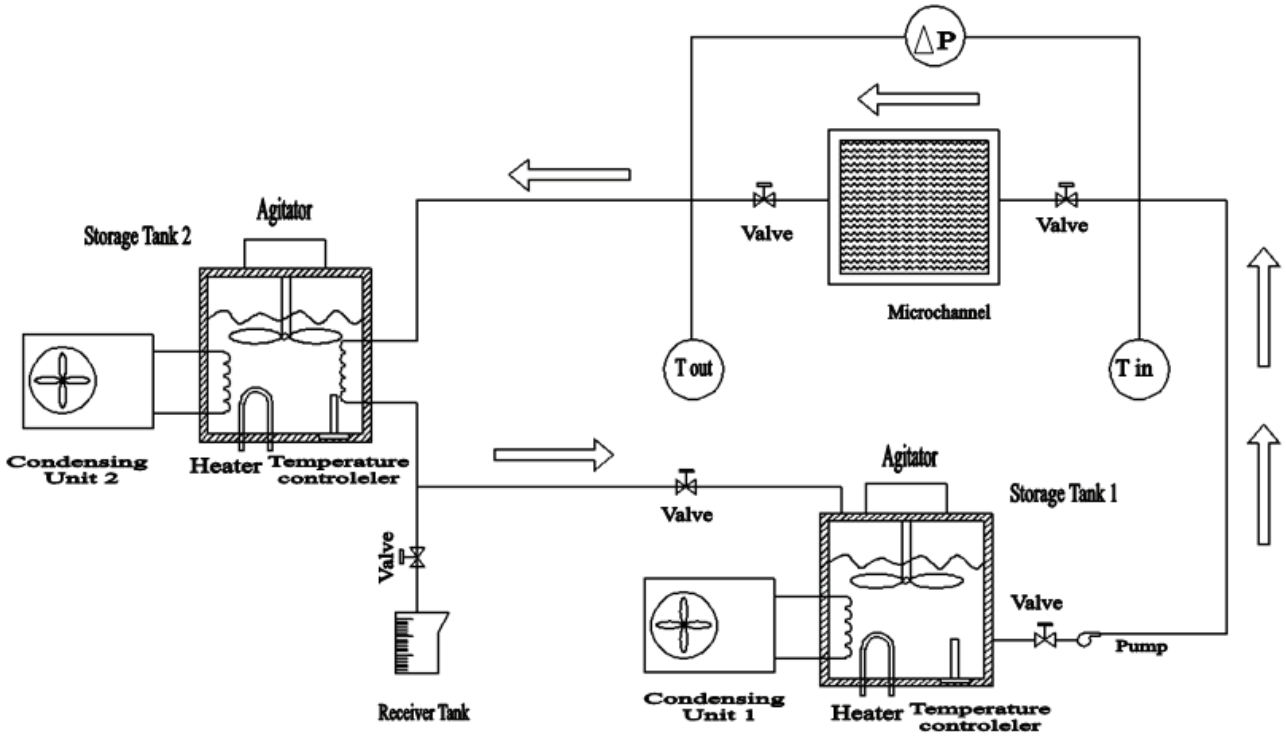


**Figure 1.** Experimental configuration.

Heat transfer rate of fluid is calculated by using following equations

$$Q = \dot{m} C_p \Delta T$$

$\dot{m}$ = mass flow rate of fluid  Cp = Specific heat of fluid

$$\Delta T = T_o - T_i$$

$T_o$ = Outlet fluid temperature; $T_i$ = Inlet fluid temperature

$$\dot{m} = \rho A V$$

$$Q = hA\,\Delta T \text{ ;watt}$$

h =Coefficient of convective heat transfer

$$A = (2H + W) \times L \times n \text{ mm}^2$$

$$\Delta T = T_w - T_f$$

$T_w$ = wall temperature; $T_f$ = Fluid temperature

$$T_f = \frac{T_i + T_o}{2}$$

$$h = \frac{Q}{A \Delta T}$$

$$Nu = \frac{h D_h}{K_f}$$

$K_f$ = 0.6 for Deionized water

$$R_e = \frac{\rho V D h}{\mu}$$

$$D_h = 4A_c / P_c$$

$A_c$= Cross section of Channel; $P_c$=Perimeter of Channel

## RESULTS AND DISCUSSION

**Grid Independent Study for CFD Analysis**

For GSF analysis a rectangular microchannel of aluminum with dimensions of 100 x 20 x 5 was used.

From table 1, it is found that deviation in pressure drop of fluid for GSF 5 and 6 is 0.12% which will be in acceptable region.

**Comparison of Straight Channel and Wave Channel**

From table 2 it is found that, as Reynolds number increases ratio of Nusselt number and ratio of pressure drop of wavy to straight microchannel get increase. Also it is found that wavy microchannel having more heat transfer rate as compare to straight channel but it increases the pressure drop which leads to increase in pumping power.

**Comparıson of Wavy Channel Without Cross Cut Verses Wavy Channel with Cross Cut**

In long microchannel, to avoid the boundary formation and to increase heat transfer rate cross cut are use at suitable distance from header.

From table 3, it is found that by using cross cut in microchannel, Nusselt number is increased by 23.91% which

**Table 1.** Variation of pressure drop at different GSF

| Length of channel | Pressure in Pa | | | | | |
|---|---|---|---|---|---|---|
| | GSF1 | GSF2 | GSF3 | GSF4 | GSF5 | GSF6 |
| 0 | 1070.12 | 1586.13 | 1887.21 | 2050.83 | 2953.17 | 2949.51 |
| 0.011 | 964.113 | 1414.47 | 1682.22 | 1818.75 | 2621.5 | 2627 |
| 0.022 | 836.923 | 1238.38 | 1473.3 | 1599.59 | 2288.64 | 2296.64 |
| 0.033 | 705.611 | 1061.3 | 1263.72 | 1365.62 | 1959.87 | 1970.04 |
| 0.044 | 588.872 | 888.837 | 1054.96 | 1138.82 | 1646.31 | 1646.31 |
| 0.055 | 473.792 | 710.471 | 841.363 | 907.13 | 1316.38 | 1316.38 |
| 0.066 | 348.004 | 533.429 | 632.366 | 683.069 | 991.68 | 991.68 |
| 0.077 | 230.83 | 357.476 | 417.655 | 454.697 | 657.311 | 657.311 |
| 0.088 | 122.027 | 176.33 | 209.715 | 224.078 | 332.979 | 332.979 |
| 0.1 | 6.25478 | 5.63502 | 2.48343 | 0.30512 | 0.024518 | 0.024518 |
| ▲P | 1063.865 | 1580.495 | 1884.727 | 2050.525 | **2949.485** | **2953.101** |

**Table 2.** Results for wavy channel and straight channel

| *Re* | *Wavy channel* | | *Straight Channel* | | *Nuw / Nus* | *ΔP w /ΔPs* |
|---|---|---|---|---|---|---|
| | *Nu* | *ΔP* | *Nu* | *ΔP* | | |
| **100** | 13.37469 | 10.3826 | 12.21994 | 7.8952 | 1.094498 | 1.315052 |
| **200** | 16.81604 | 27.8786 | 13.52655 | 19.3978 | 1.243188 | 1.437204 |
| **300** | 20.49224 | 46.1372 | 15.4569 | 30.2703 | 1.325767 | 1.524174 |
| **400** | 20.98664 | 81.1107 | 14.84987 | 49.4699 | 1.413254 | 1.639597 |
| **500** | 22.34093 | 115.175 | 15.26989 | 66.9503 | 1.463071 | 1.720306 |
| **600** | 23.0582 | 133.053 | 15.56244 | 75.7904 | 1.481657 | 1.755539 |
| **700** | 23.76555 | 167.351 | 15.76818 | 92.2487 | 1.507184 | 1.814129 |
| **800** | 24.02657 | 203.692 | 15.70297 | 109.112 | 1.530066 | 1.866816 |
| **900** | 24.34162 | 241.856 | 15.77634 | 126.296 | 1.542919 | 1.914993 |

**Table 3.** CFD results of wavy channel without cross cut verses wavy channel with crosscut

| Channel | Re | V | Heat Flux | Ti | To | Tf | Tw | *ΔP* | *Nu* |
|---|---|---|---|---|---|---|---|---|---|
| **Without Cross Cut** | 500 | 0.38 | 20000 | 299.99 | 303.36 | 301.6 | 303.96 | 1609.11 | 16.31 |
| **With Cross Cut** | 500 | 0.38 | 20000 | 303.92 | 301.96 | 304.2 | 303.9 | 2159.73 | 20.21 |

indicate that cross cut microchannel is having more heat transfer rate than that of straight channel. But simultaneously it increases the pressure drop which leads to increase in pumping power.

**Optimization of Geometry**

For present research work, cross cut microchannel was used hence it is important to optimize the geometry of it. Initially the angle of cross cut is finalized by simulating different geometries of cross cut angle 00, 100, 200, 300, 400 and 500 with the help of Computational fluid dynamics (CFD). For simulation, geometry of dimension 100 x 20 x 5 is used. This geometry is simulate by applying following fluent parameters. Table 4 shows parameter which to be used for the CFD simulation.

**Variation of Temperature with Change in Cross Cut Angle**

Following figures showing temperature distribution in microchannel with different cross cut angles.

Figure 2 to Figure 15 is showing temperature distribution and temperature chart for microchannel without cross cut and with cross cut with cross cut angle 0°, 10°, 20°, 30°, 40° and 50° respectively. All geometries are simulated

**Table 4.** Fluent parameter

| Parameters | Conditions | Value |
|---|---|---|
| GSF | - | 6 |
| Mesh scale | Mm | - |
| Mesh type | Tetra mix | - |
| Model | Energy on | - |
| Solid material | Aluminum | - |
| Fluid material | Water- liquid | - |
| Cell zone condition liquid | Water- liquid | - |
| Cell zone conditions Solid | Aluminum | - |
| Boundary conditions Inlet | Velocity inlet | 0.38 m/s (For Re 500 ) |
| Outlet | Pressure-outlet | Zero gauge pressure |
| Heaters | Wall type | Heat flux: 20000 W/m$^2$ |
| Reference value | Compute from inlet | - |
| Solution initialization | Compute from inlet | - |
| Run calculation | Iteration | 1000 |

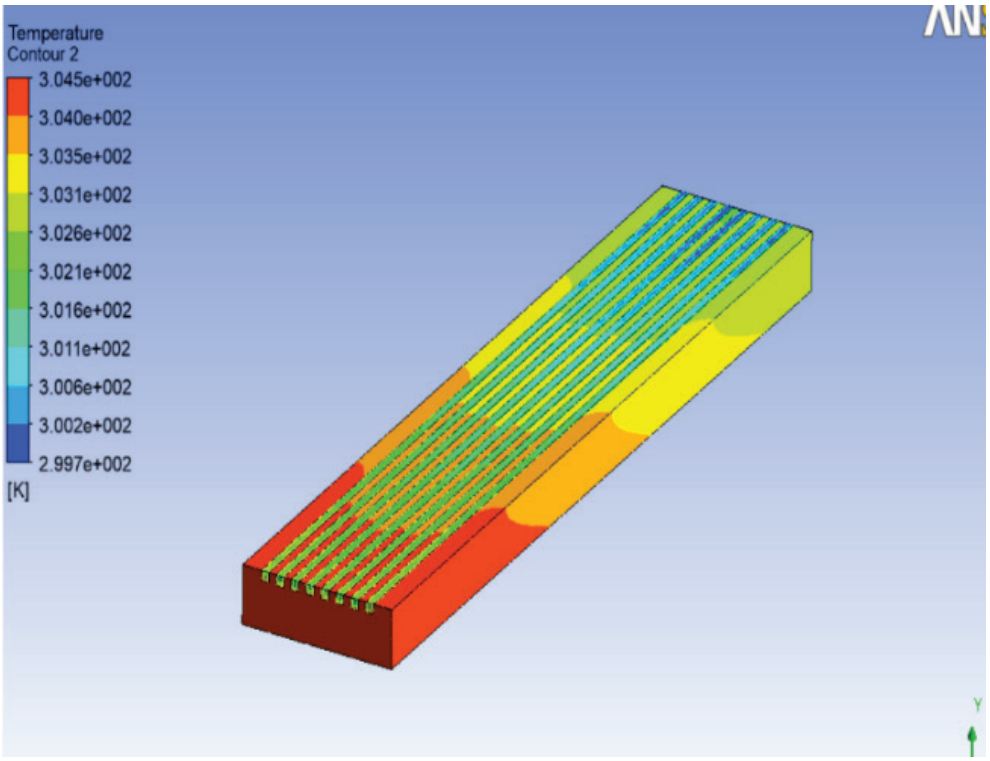


**Figure 2.** Temperature distribution without cross cut.

at Reynolds number 500 and constant heat flux of 20000 w/m$^2$. Corresponding temperature at different location is measured as shown in Table 5.

From Table 5, it is observed that for given operating condition geometry with cross cut angle 30° showing more temperature difference than plane geometry and other cross cut geometry.

**Variation of Pressure with change in Cross Cut Angle**

Figure 16 to Figure 29 are showing pressure distribution and pressure chart in microchannel for without cross cut and different cross cut angles.

From Table 6, it is observed that pressure drop is slightly increased in cross cut microchannel which caused increase in pumping power. Maximum increase in pressure drop

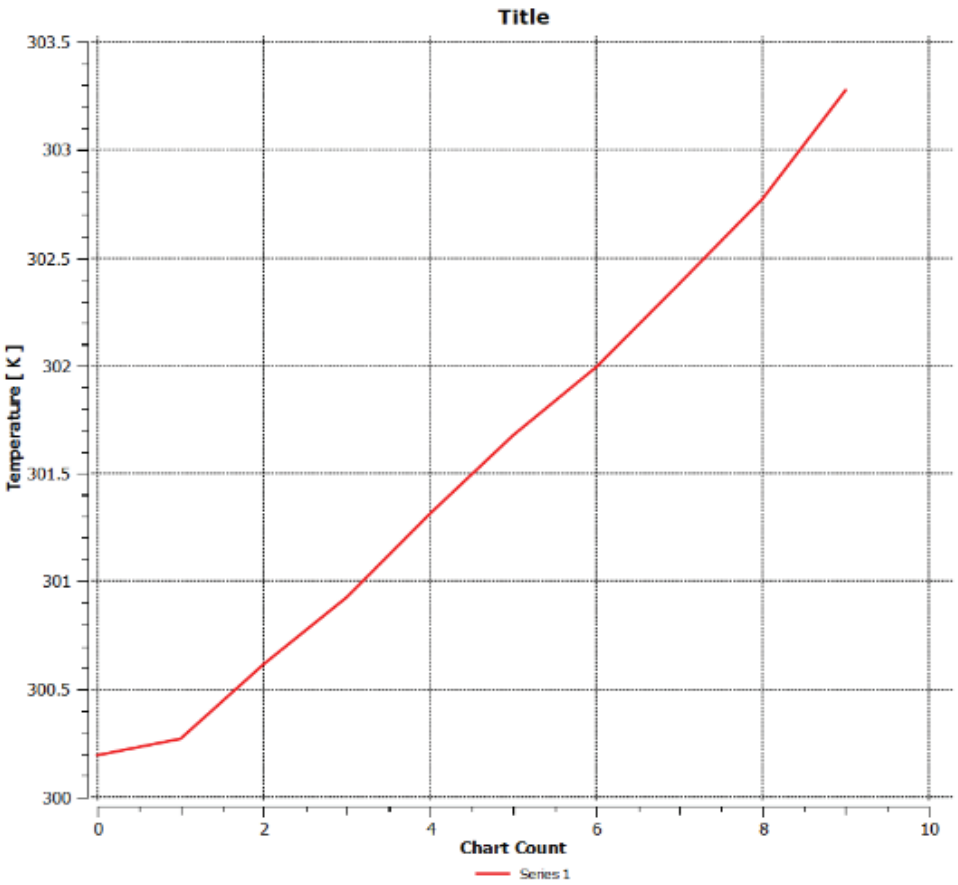


**Figure 3.** Temperature chart of without cross cut.

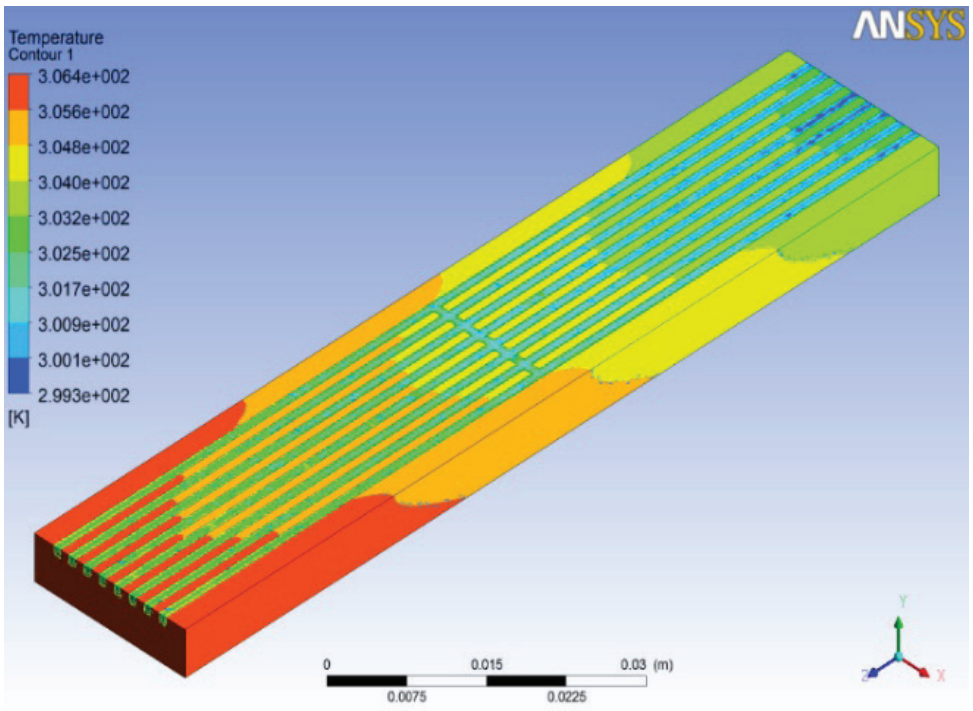


**Figure 4.** Temperature distribution with cross cut 0°.

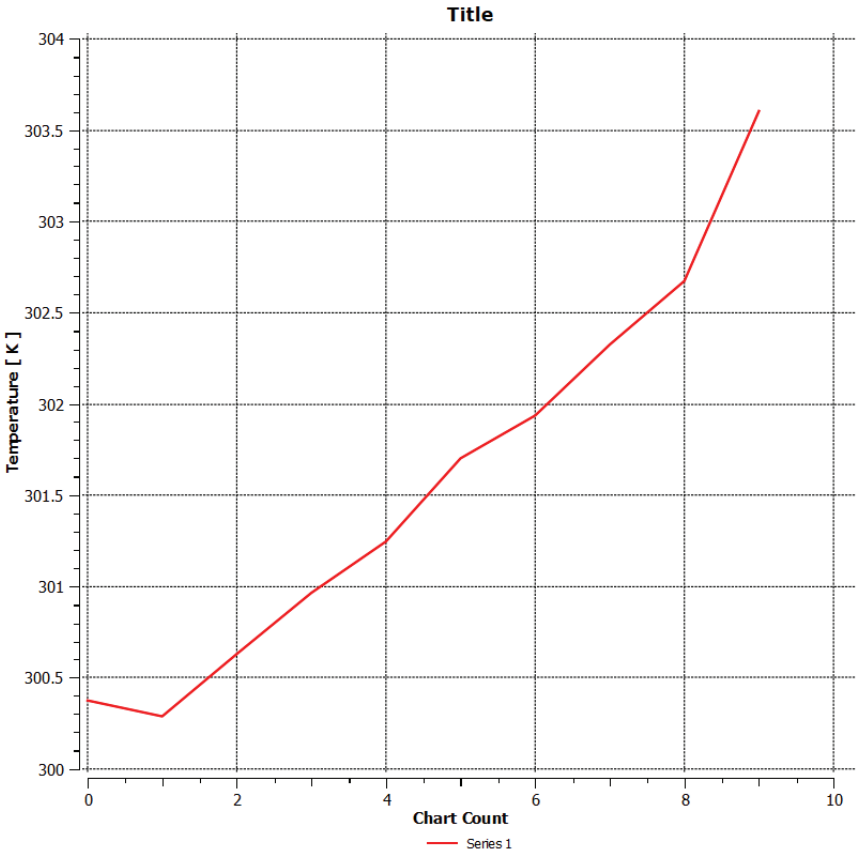


**Figure 5.** Temperature chart of cross cut 0°.

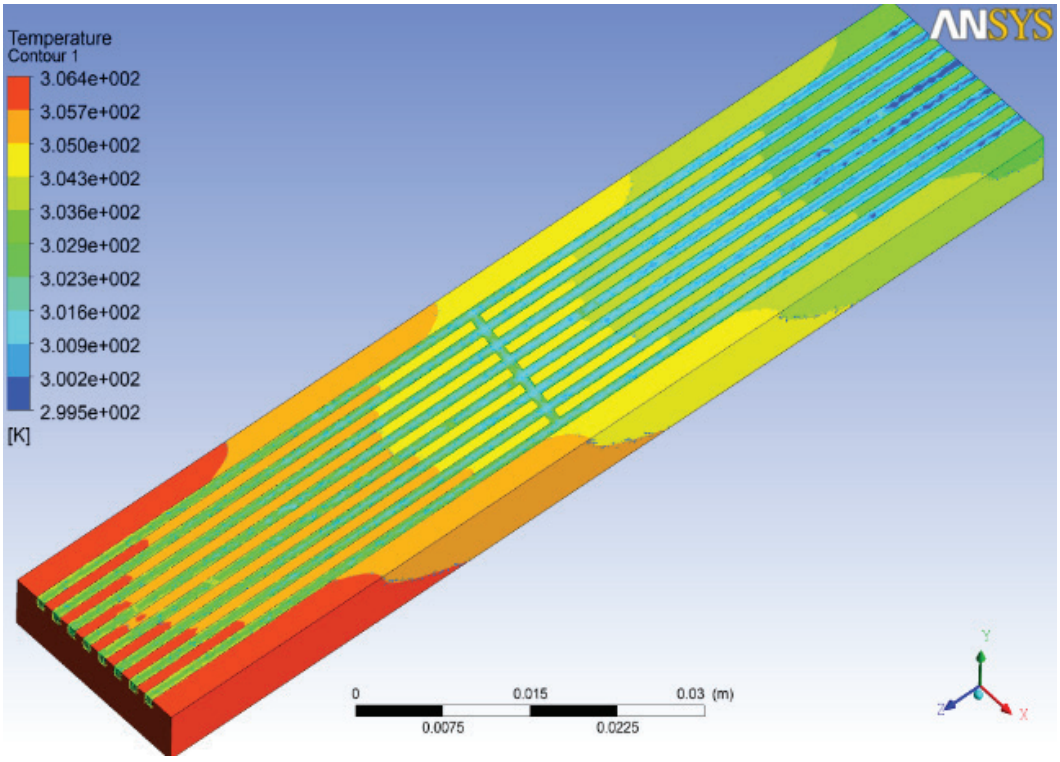


**Figure 6.** Temperature distribution with cross cut 10°.

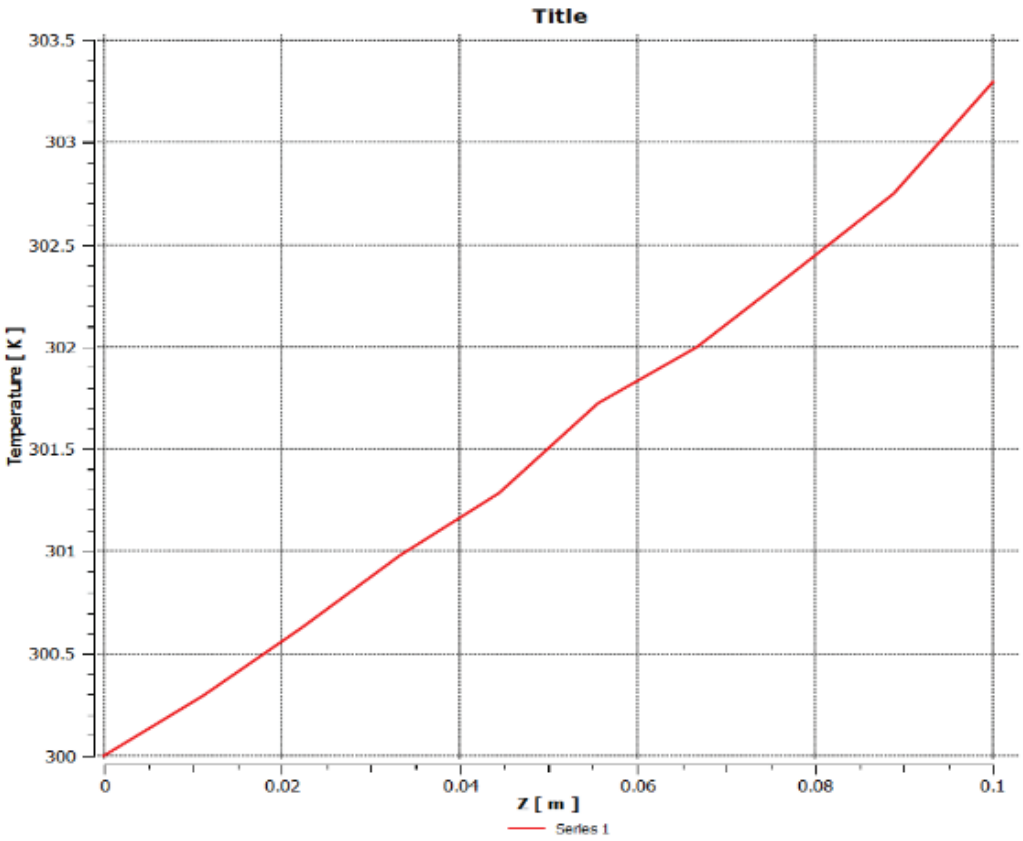


**Figure 7.** Temperature chart of cross cut 10°.

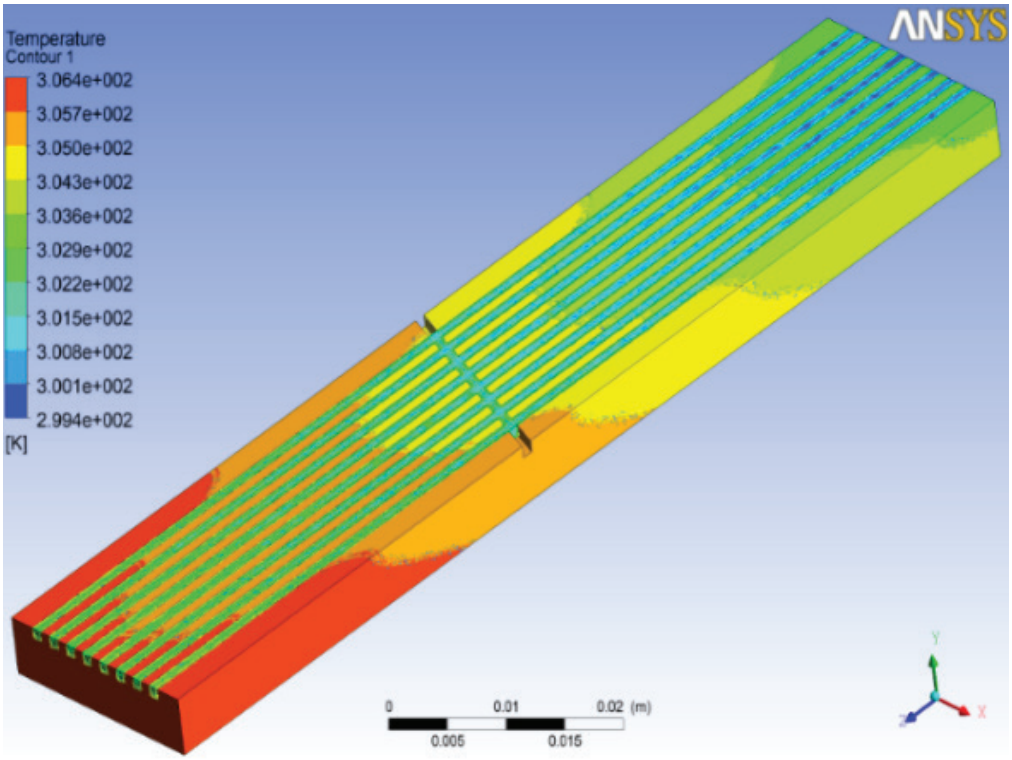


**Figure 8.** Temperature distribution with cross cut 20°.

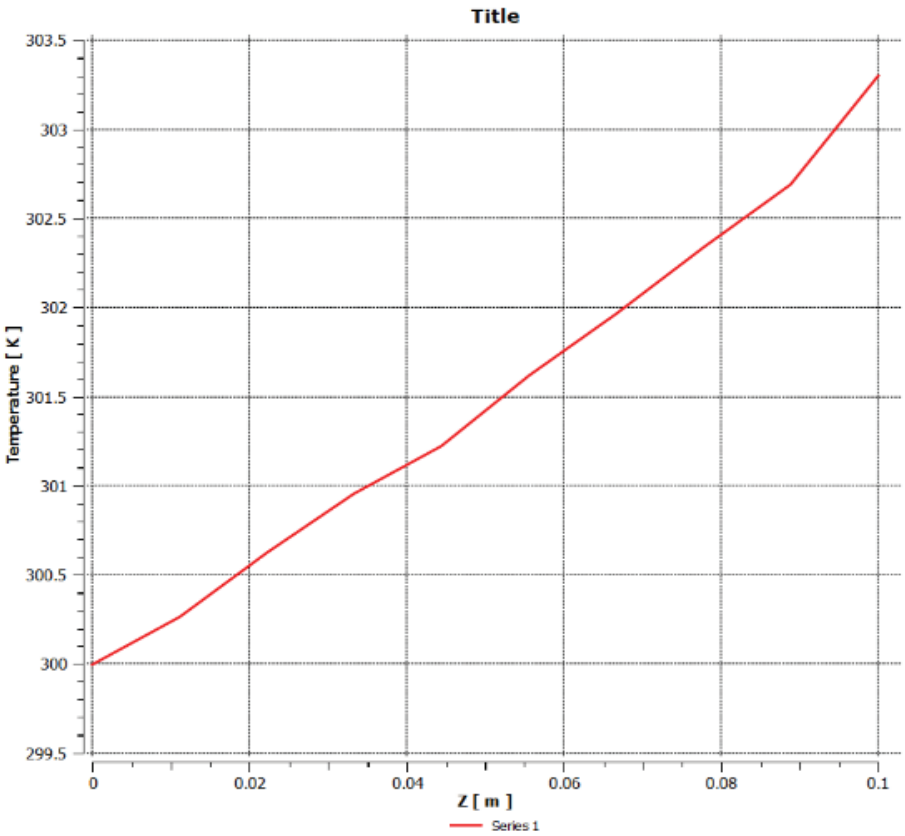


**Figure 9.** Temperature chart of cross cut 20°.

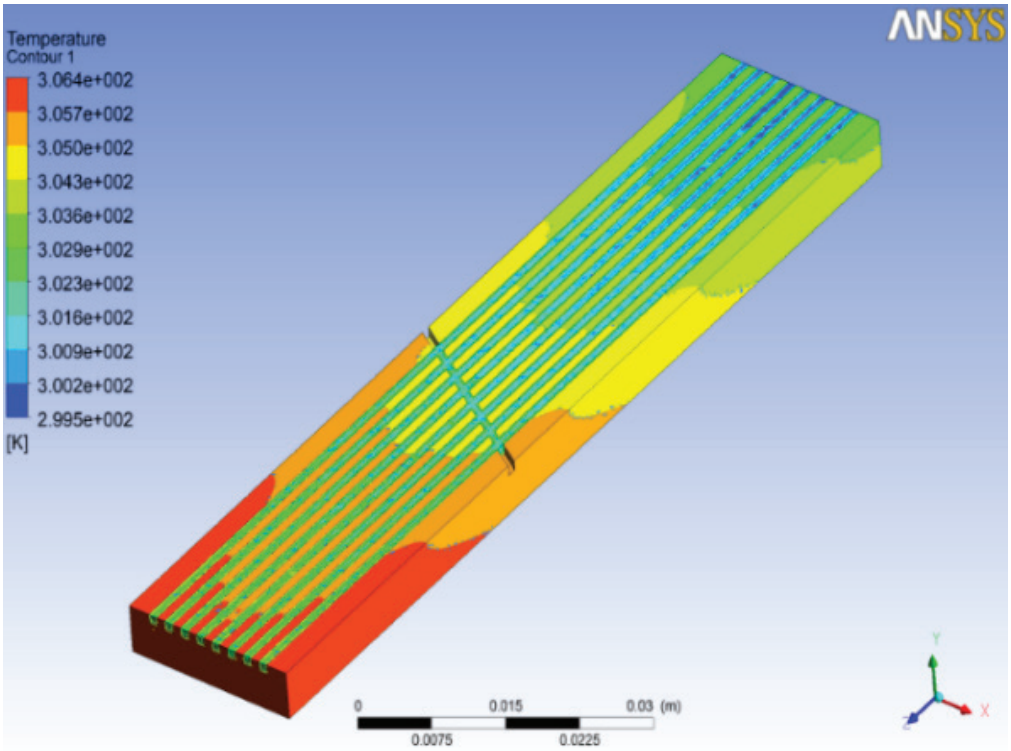


**Figure 10.** Temperature distribution with cross cut 30°.

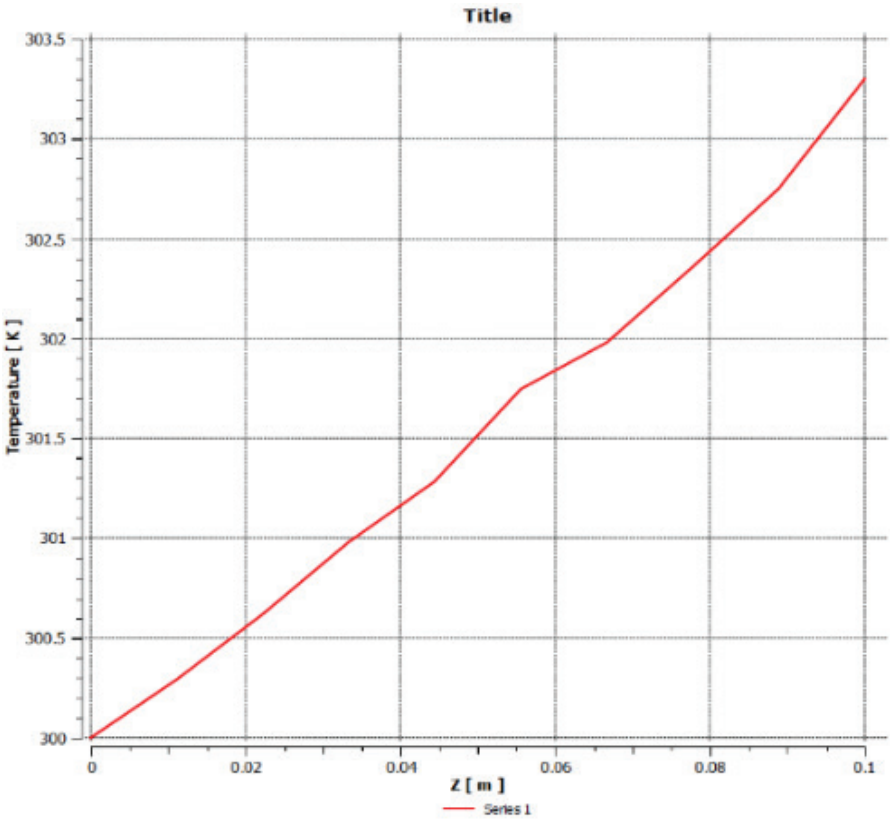


**Figure 11.** Temperature chart of cross cut 30°.

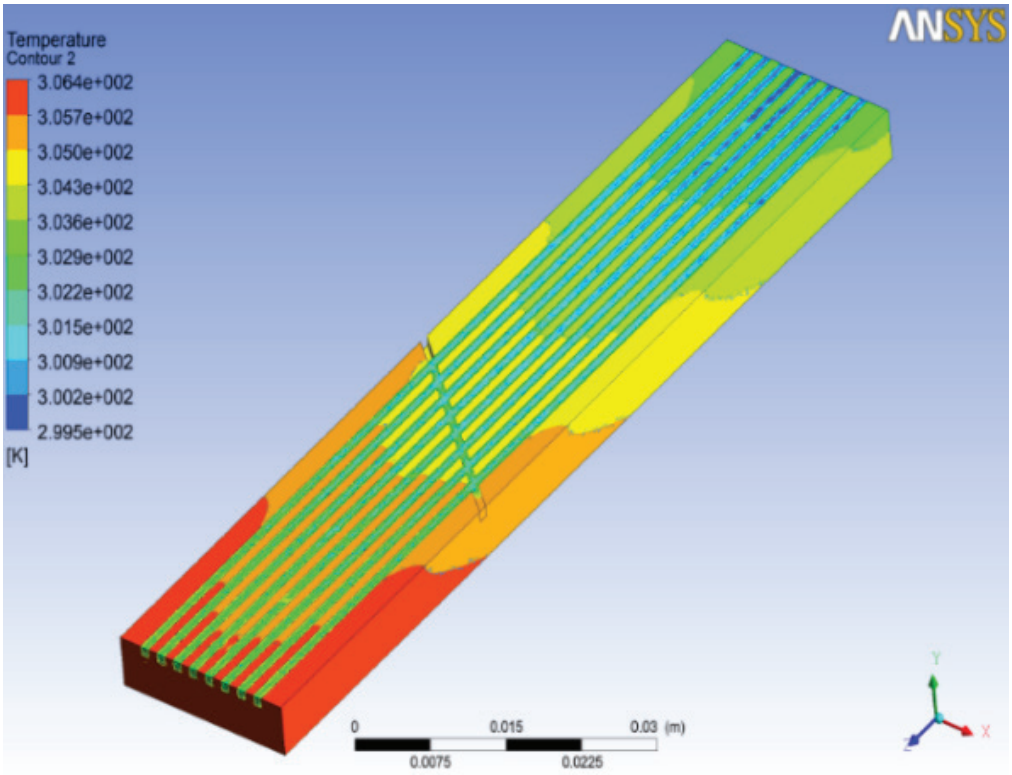


**Figure 12.** Temperature distribution with cross cut 40°.

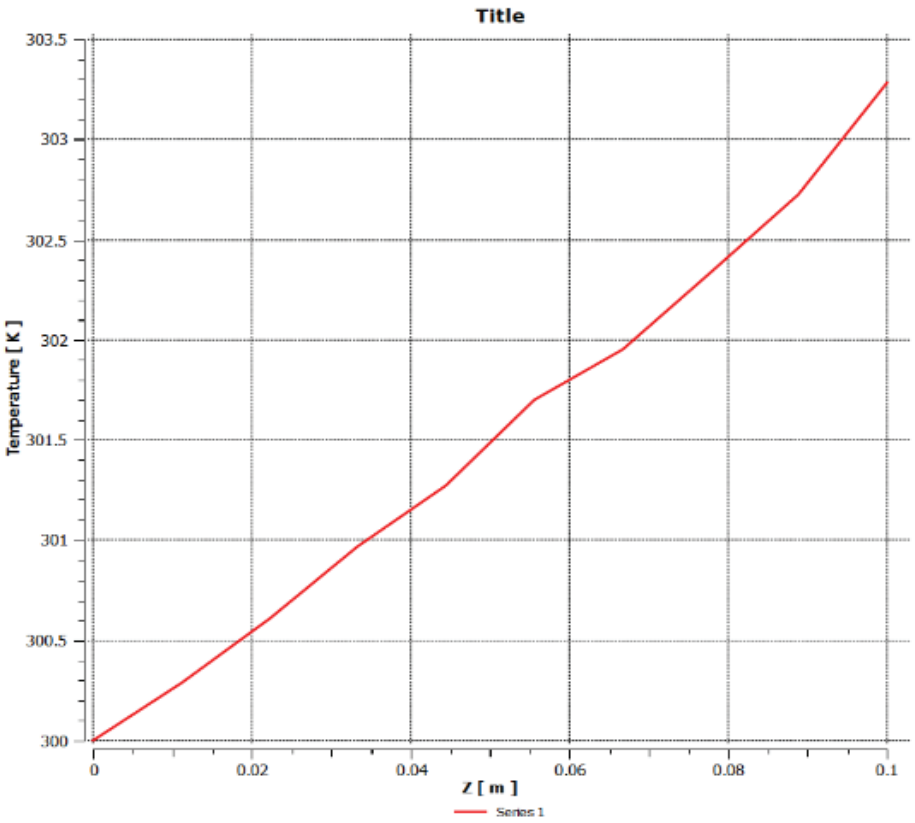


**Figure 13.** Temperature chart of cross cut 40°.

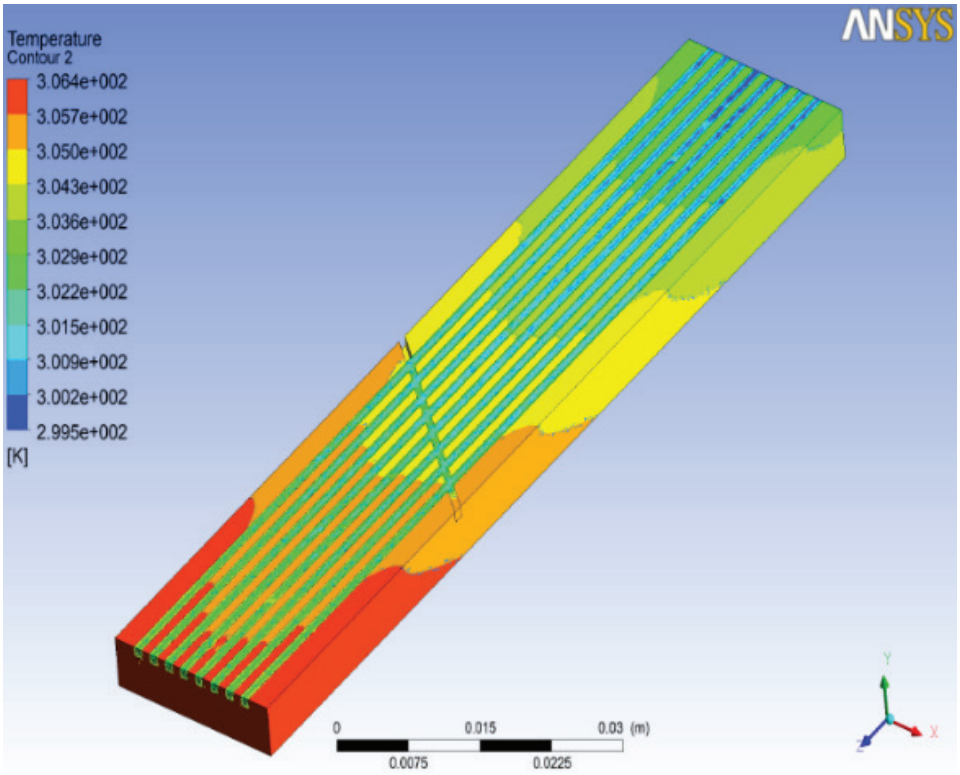


**Figure 14.** Temperature distribution with cross cut 50°.

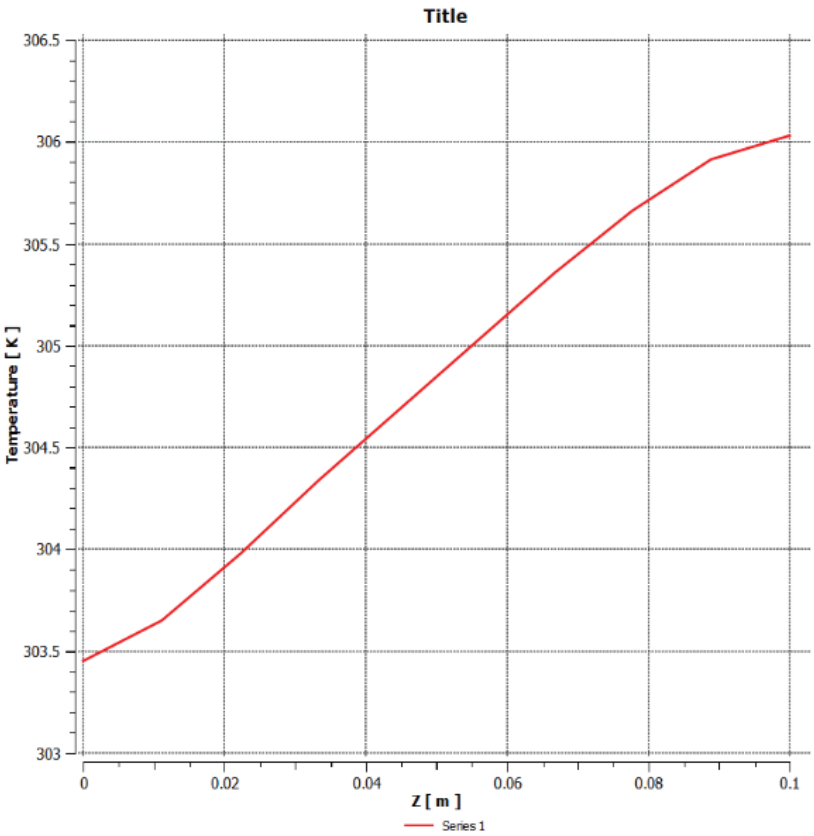


**Figure 15.** Temperature chart of cross cut 50°.

**Table 5.** Temperature distribution in microchannel with different crosscut angle

| Distance | Temperature in K | | | | | | |
|---|---|---|---|---|---|---|---|
| | **Without cut** | **273K** | **283K** | **293K** | **303K** | **313K** | **323K** |
| 0.000 | 300.192 | 300.376 | 300 | 299.999 | 300 | 300 | 300 |
| 0.011 | 300.272 | 300.289 | 300.295 | 300.267 | 300.295 | 300.286 | 300.284 |
| 0.022 | 300.614 | 300.628 | 300.627 | 300.624 | 300.624 | 300.607 | 300.6207 |
| 0.033 | 300.925 | 300.964 | 300.981 | 300.953 | 300.981 | 300.969 | 300.9622 |
| 0.044 | 301.312 | 301.243 | 301.285 | 301.225 | 301.283 | 301.273 | 301.2702 |
| 0.056 | 301.678 | 301.699 | 301.721 | 301.615 | 301.747 | 301.699 | 301.6932 |
| 0.067 | 301.996 | 301.937 | 302 | 301.968 | 301.982 | 301.951 | 301.9723 |
| 0.078 | 302.382 | 302.327 | 302.366 | 302.331 | 302.357 | 302.331 | 302.349 |
| 0.089 | 302.771 | 302.675 | 302.748 | 302.687 | 302.75 | 302.725 | 302.726 |
| 0.100 | 303.170 | 303.536 | 303.296 | 303.297 | 303.303 | 303.286 | 303.223 |
| ▲T | 2.988 | 3.15 | 3.296 | 3.298 | 3.303 | 3.286 | 3.223 |

of 4.66% is observed corresponding to 0° cross cut. Also increased in pressure drop corresponding to 30° is 2.4%

**Wall Temperature of Cross Cut Microchannel**

From Table 7, it is observed that wall temperature of all cross cut geometry are nearly same as applied heat flux is constant and thickness of channel is small. In the context of microchannels, the wall temperature refers to the temperature of the surfaces forming the boundaries of the channel. In a cross-cut microchannel, typically having a rectangular or square cross-section, the wall temperature is crucial in determining heat transfer characteristics. Factors influencing the wall temperature include fluid

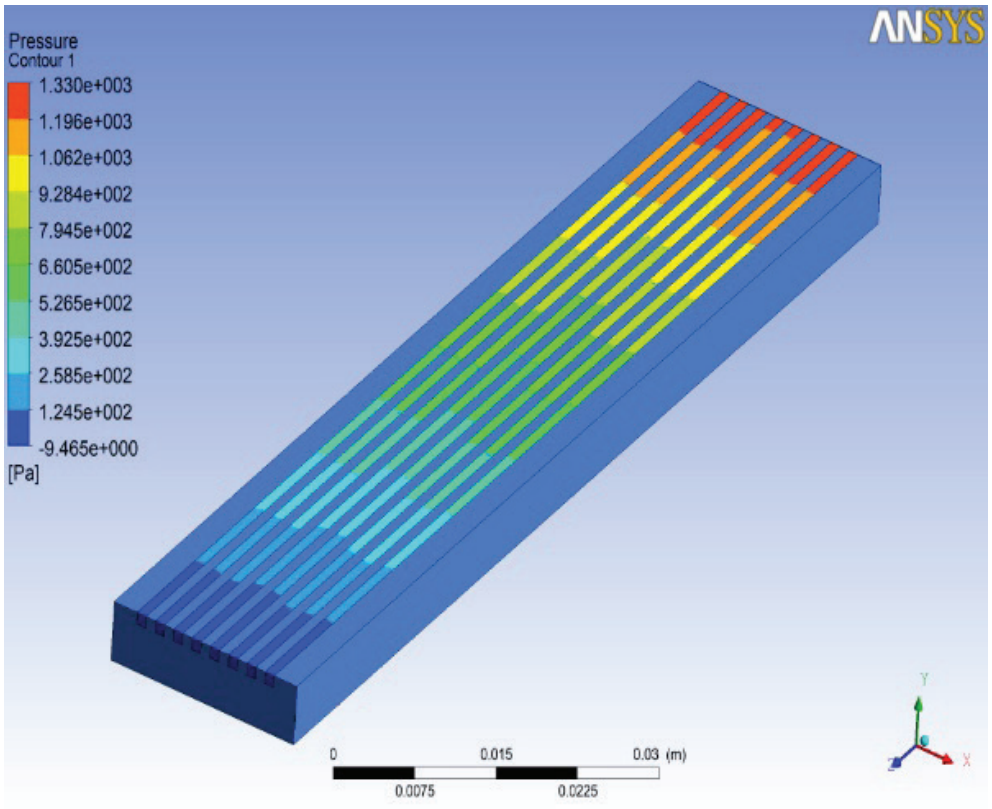


**Figure 16.** Pressure distribution without cross cut.

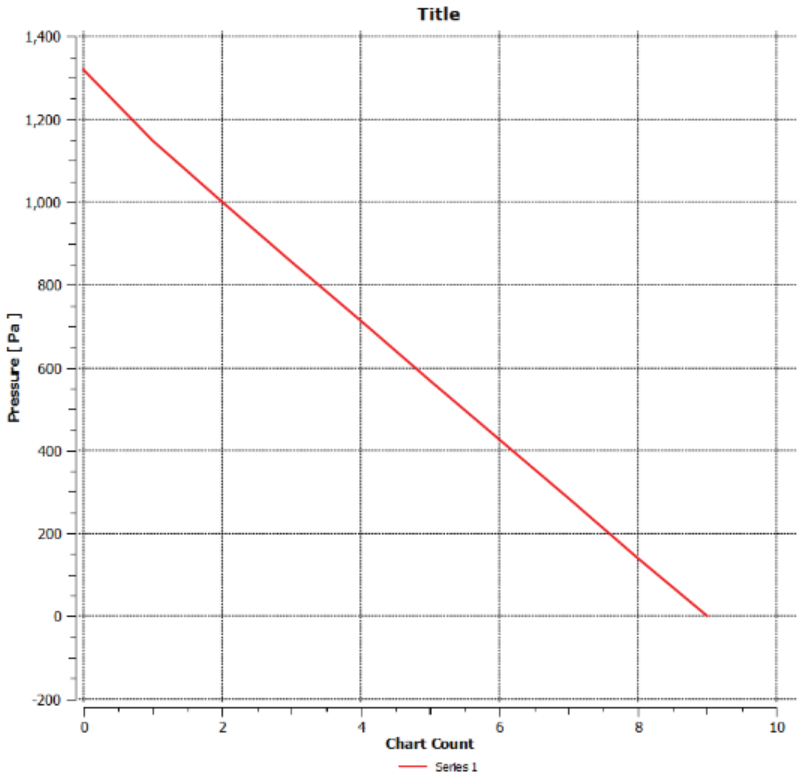


**Figure 17.** Pressure chart without cross cut.

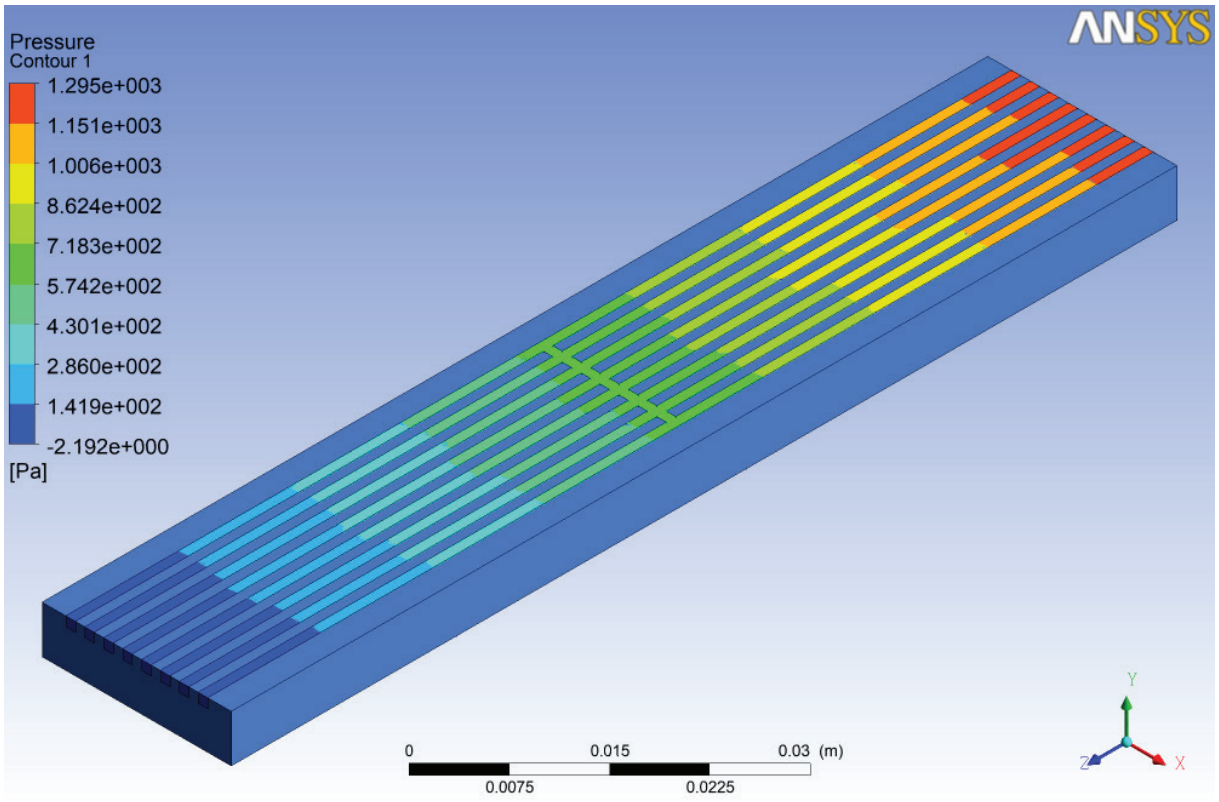


**Figure 18.** Pressure distribution with cross cut 0°.

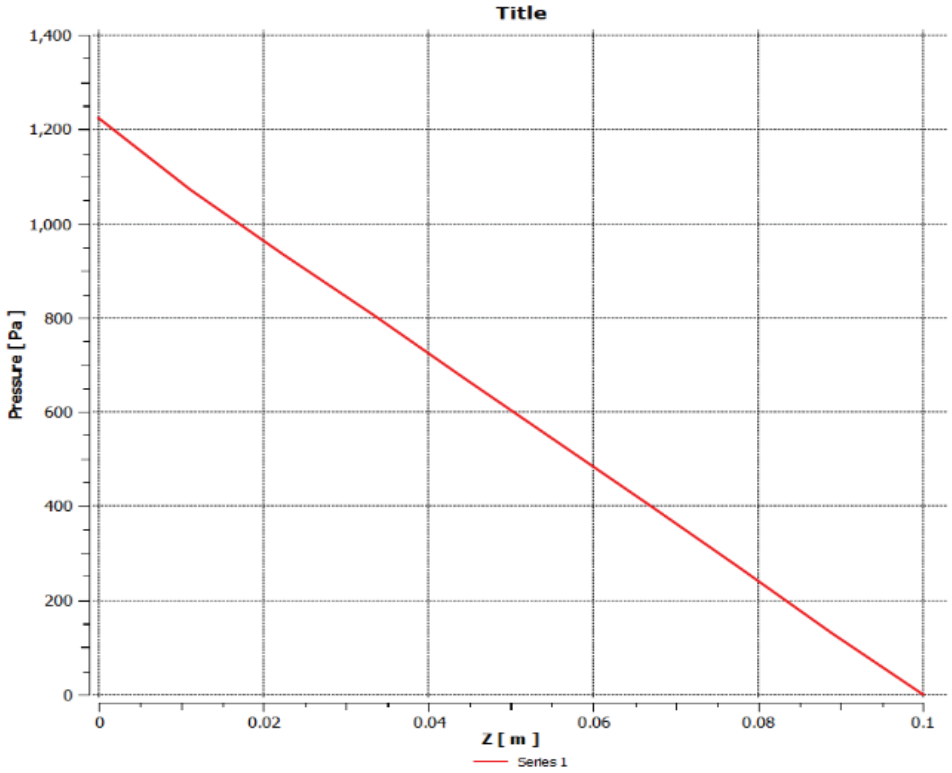


**Figure 19.** Pressure chart of cross cut 0°.

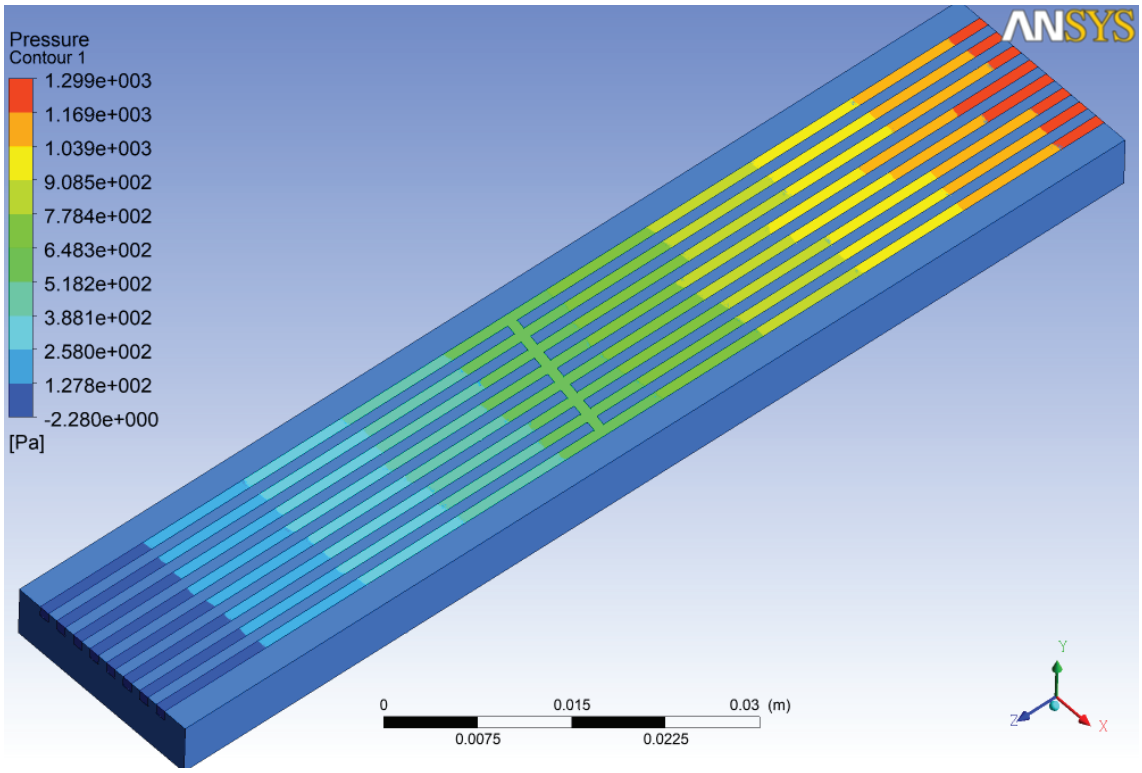


**Figure 20.** Pressure distribution with cross cut 10°.

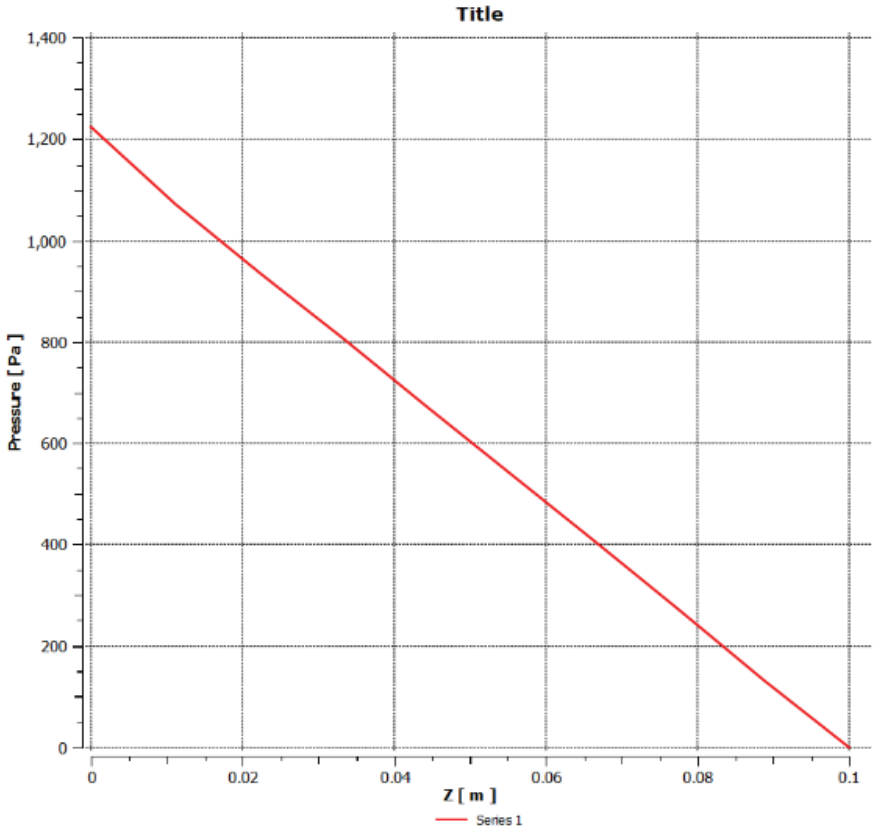


**Figure 21.** Pressure chart of cross cut 10°.

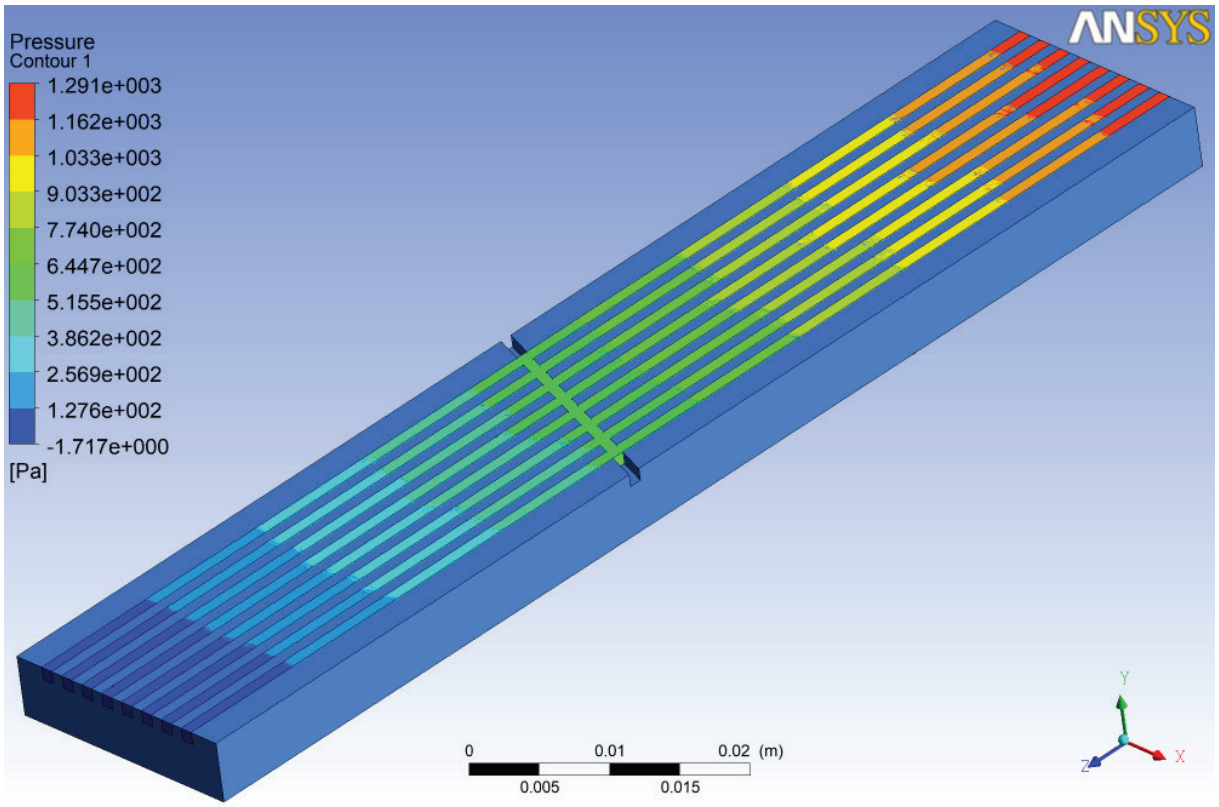


**Figure 22.** Pressure distribution with cross cut 20°.

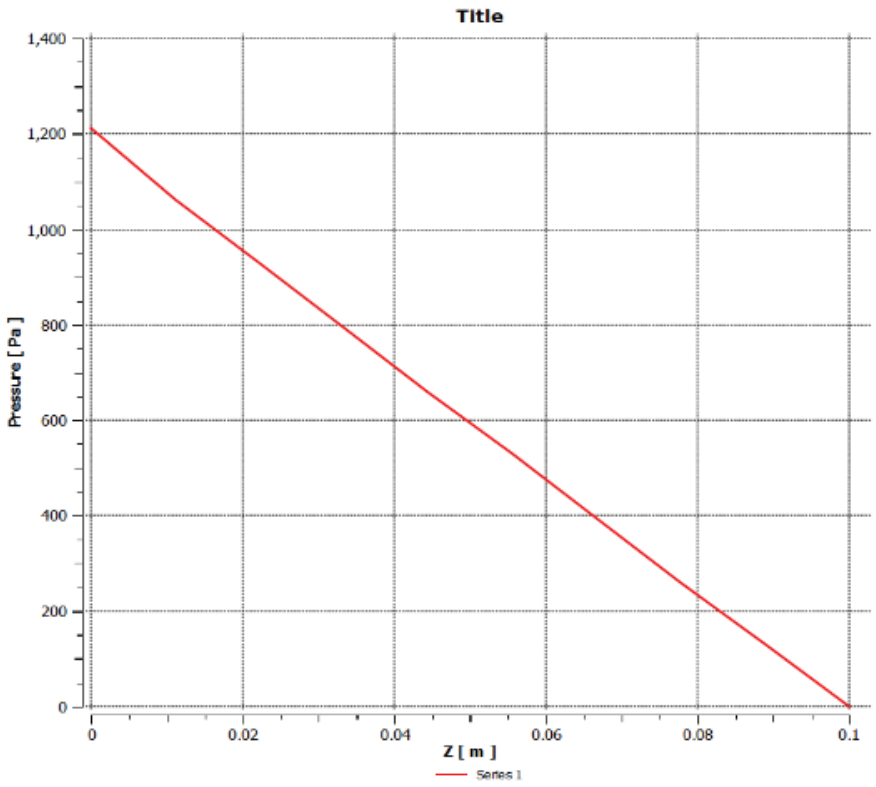


**Figure 23.** Pressure chart of cross cut 20°.

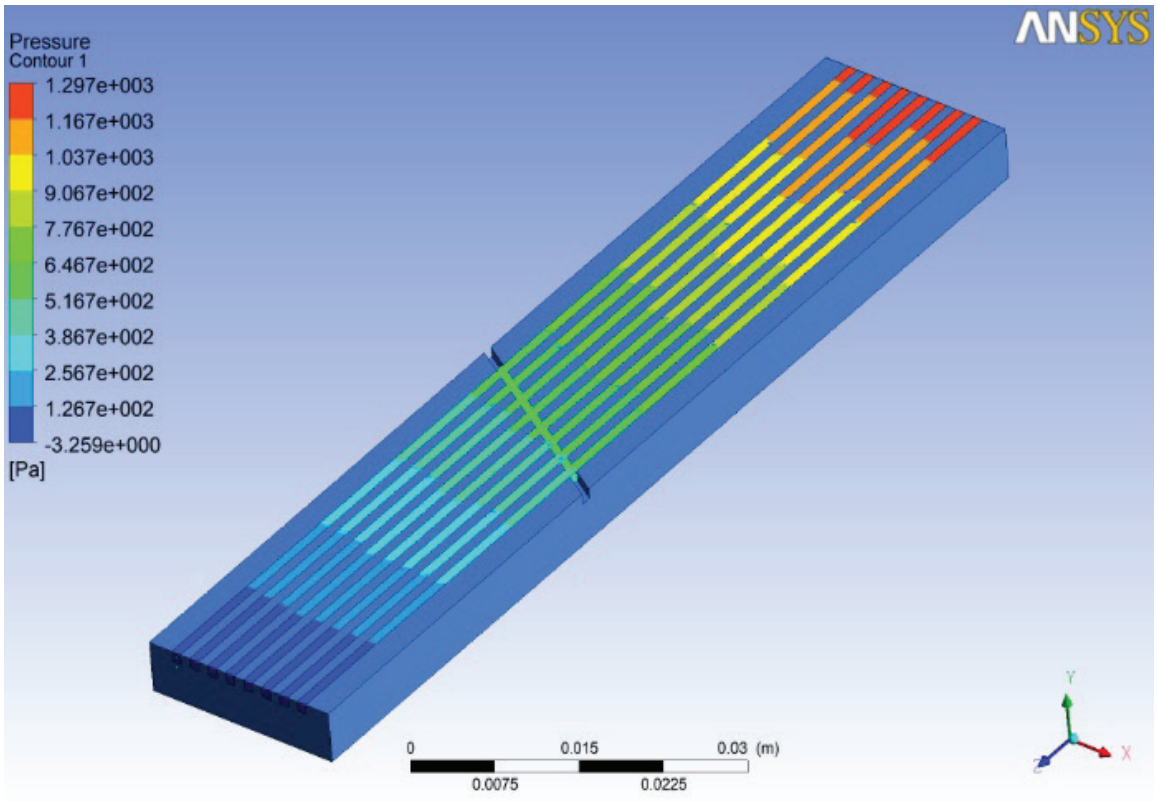


**Figure 24.** Pressure distribution with cross cut 30°.

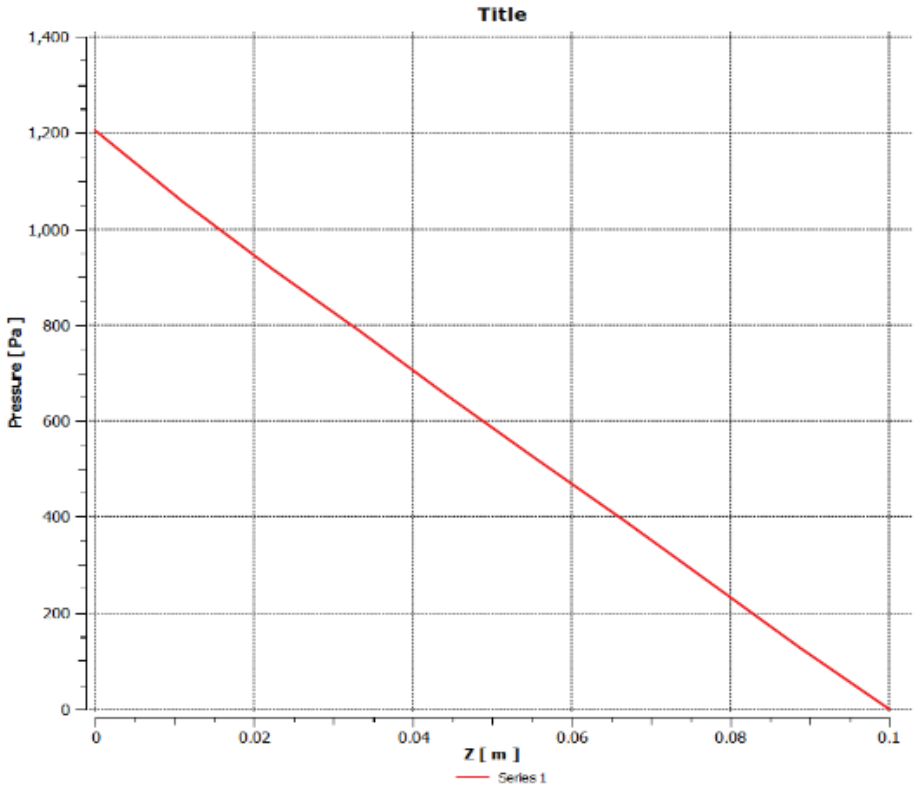


**Figure 25.** Pressure chart of cross cut 30°.

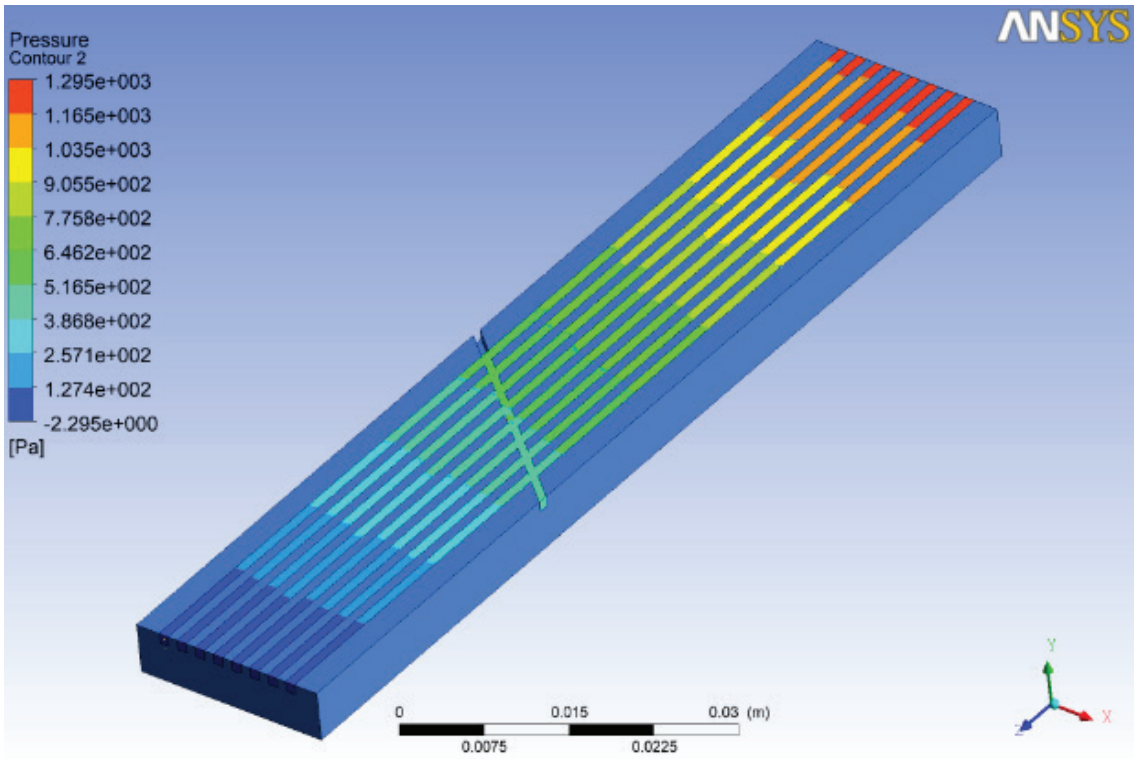


**Figure 26.** Pressure distribution with cross cut 40°.

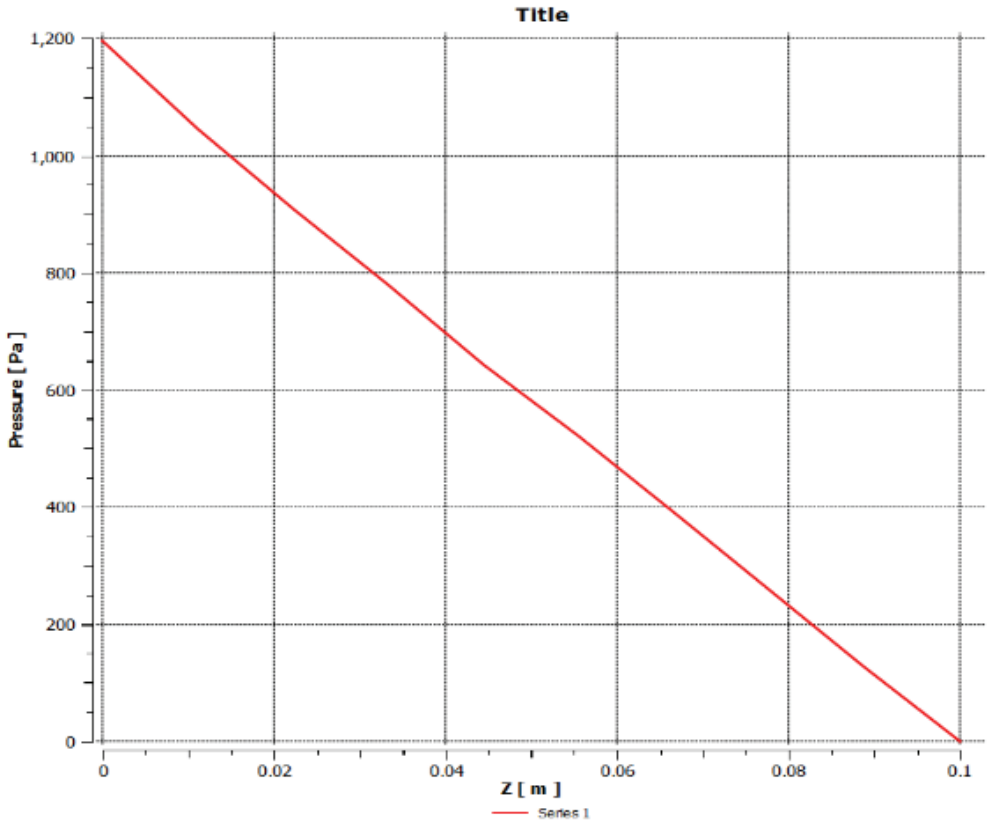


**Figure 27.** Pressure chart of cross cut 40°.

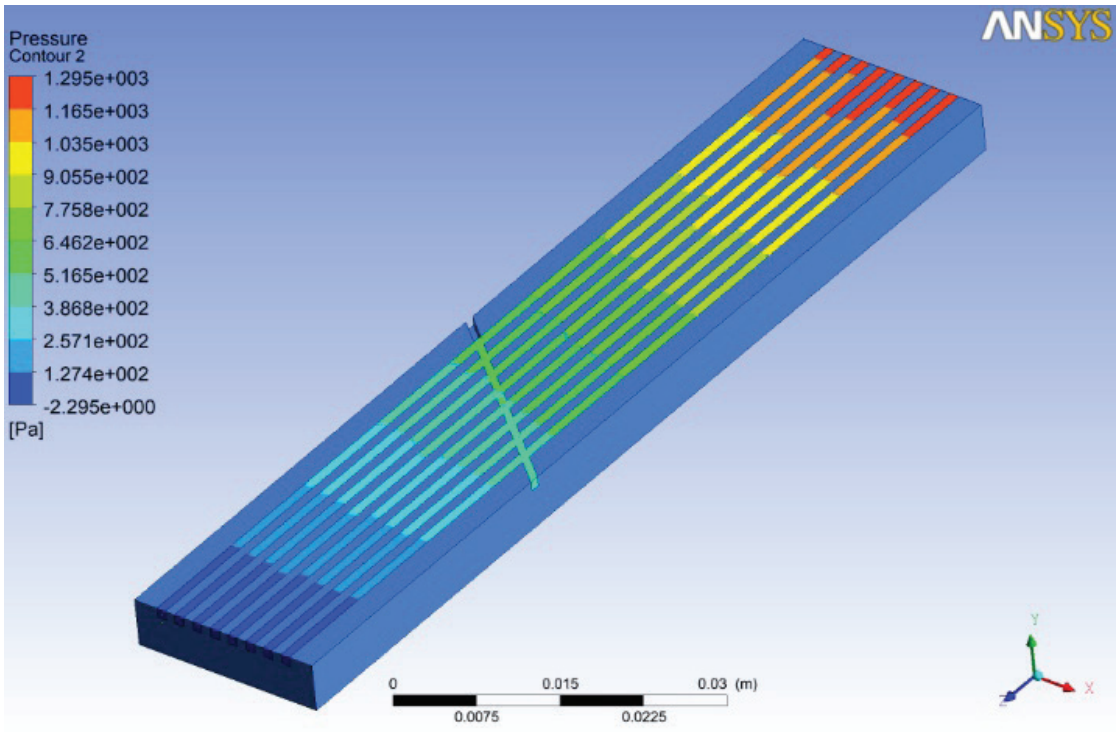


**Figure 28.** Pressure distribution with cross cut 50°.

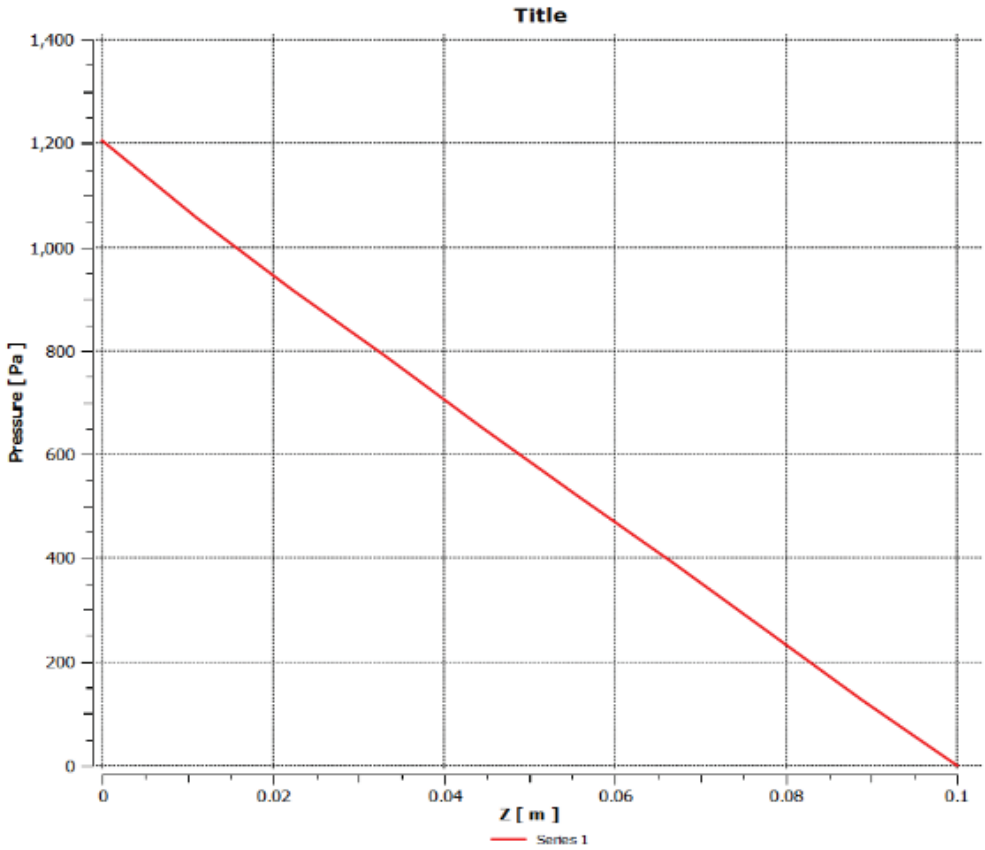


**Figure 29.** Pressure chart of cross cut 50°.

**Table 6.** Pressure distribution in microchannel with different crosscut angle

| Distance | Pressure in Pa | | | | | | |
|---|---|---|---|---|---|---|---|
| | **Without cut** | **00** | **100** | **200** | **300** | **400** | **500** |
| 0 | 1170.73 | 1229.06 | 1223.72 | 1211.52 | 1200.56 | 1196.25 | 1220.14 |
| 0.011 | 1108.98 | 1077.09 | 1072.69 | 1063.45 | 1054.53 | 1045.86 | 1076.767 |
| 0.022 | 1001.14 | 941.569 | 935.974 | 929.277 | 917.804 | 909.363 | 939.1878 |
| 0.033 | 856.936 | 811.446 | 805.856 | 795.768 | 787.687 | 779.313 | 806.1677 |
| 0.044 | 714.789 | 674.545 | 670.549 | 659.234 | 652.392 | 643.952 | 669.2435 |
| 0.056 | 570.088 | 538.259 | 536.621 | 529.616 | 521.666 | 521.344 | 536.2657 |
| 0.067 | 428.066 | 404.154 | 403.181 | 394.525 | 391.913 | 389.544 | 401.8972 |
| 0.078 | 285.643 | 268.983 | 268.544 | 261.473 | 261.064 | 259.459 | 267.5277 |
| 0.089 | 139.307 | 130.64 | 130.232 | 131.196 | 126.737 | 125.965 | 130.6795 |
| 0.1 | -0.00999 | 0.591988 | 0.068479 | 0.17566 | 0.064067 | 0.063416 | 0.158937 |
| ▲P | 1170.74 | 1228.468 | 1223.652 | 1211.344 | 1200.496 | 1196.187 | 1219.981 |

**Table 7.** Wall temperature distribution in microchannel with different crosscut angle

| Distance | Wall Temperature in 0K | | | | | | |
|---|---|---|---|---|---|---|---|
| | **Without cut** | **00** | **100** | **200** | **300** | **400** | **500** |
| 0 | 303.138 | 303.458 | 303.462 | 303.453 | 303.459 | 303.453 | 303.455 |
| 0.011 | 303.389 | 303.6547 | 303.659 | 303.648 | 303.657 | 303.648 | 303.651 |
| 0.022 | 303.766 | 303.998 | 303.997 | 303.999 | 303.998 | 303.981 | 303.9927 |
| 0.033 | 304.161 | 304.3573 | 304.356 | 304.359 | 304.357 | 304.334 | 304.35 |
| 0.044 | 304.528 | 304.6993 | 304.702 | 304.695 | 304.701 | 304.675 | 304.6903 |
| 0.056 | 304.889 | 305.0543 | 305.052 | 305.064 | 305.047 | 305.019 | 305.0433 |
| 0.067 | 305.254 | 305.384 | 305.386 | 305.384 | 305.382 | 305.355 | 305.3737 |
| 0.078 | 305.576 | 305.6893 | 305.689 | 305.695 | 305.684 | 305.663 | 305.6807 |
| 0.089 | 305.83 | 305.9297 | 305.933 | 305.928 | 305.928 | 305.911 | 305.9223 |
| 0.1 | 305.948 | 306.0453 | 306.049 | 306.041 | 306.046 | 306.03 | 306.039 |
| Avg.$T_w$ | 304.6479 | 304.827 | 304.8285 | 304.8266 | 304.8259 | 304.8069 | 304.8198 |

flow rate, channel material thermal conductivity, heat transfer coefficient at the fluid-wall interface, and fluid inlet temperature. Understanding the wall temperature distribution along the microchannel length and width is key for optimizing heat transfer processes like microchannel heat exchangers or microreactors. Computational fluid dynamics (CFD) simulations and experimental techniques such as infrared thermography or thermocouple measurements are used to study this distribution. Controlling wall temperature is vital for microchannel applications like microelectronics cooling, chemical synthesis, and biomedical devices. Maintaining uniform and controlled wall temperature enhances heat transfer efficiency, improves process control, and ensures device reliability and performance.

**CFD Results**

By measuring fluid temperature, pressure drop and wall temperature at various points, Nusselt number for each geometry is calculated as shown in Table 8.

It is found that Nusselt number of cross cut geometry is greater than Nusselt number of without cross cut geometry as mentioned in Table 8. It is observed that geometry of cross cut angle 30° showing maximum Nusselt number 11.497 which is 3.66% greater than that of plain geometry.

Numerous challenges in energy and geophysical industries, such as thermal insulation, geophysical flows, petroleum resources, and polymer processing, require the analysis of mixed convective thermal and solutal transport phenomena of non-Newtonian fluids in a porous medium across various geometries. Many real fluids, including cosmetic products, grease, body fluids, and others, exhibit

**Table 8.** Variation of nusselt number and pressure drop for different cross cut angle

| Parameter | Angle of cross cut | | | | | | |
|---|---|---|---|---|---|---|---|
| | **Without cross cut** | **00** | **100** | **200** | **300** | **400** | **500** |
| $\Delta T_1$ | 2.988 | 3.18 | 3.296 | 3.298 | 3.303 | 3.286 | 3.223 |
| $T_f$ | 301.7335 | 301.991 | 301.648 | 301.648 | 301.6515 | 301.643 | 301.6115 |
| Avg.$T_w$ | 304.6479 | 304.827 | 304.8285 | 304.8266 | 304.8259 | 304.8069 | 304.8198 |
| $\Delta T_2$ | 2.9144 | 2.836 | 3.1805 | 3.1786 | 3.1744 | 3.1639 | 3.2083 |
| M | 0.00038 | 0.00038 | 0.00038 | 0.00038 | 0.00038 | 0.00038 | 0.00038 |
| $C_p$ | 4187.000 | 4187.000 | 4187.000 | 4187.000 | 4187.000 | 4187.000 | 4187.000 |
| A | 0.00024 | 0.00024 | 0.00024 | 0.00024 | 0.00024 | 0.00024 | 0.00024 |
| Q | 4.738 | 4.8211 | 5.244 | 5.247 | 5.255 | 5.228 | 5.128 |
| H | 6654.834 | 6855.766 | 6870.164 | 6878.442 | 6897.985 | 6885.257 | 6659.792 |
| **Nu** | **11.090** | **11.426** | **11.450** | **11.464** | **11.497** | **11.475** | **11.100** |

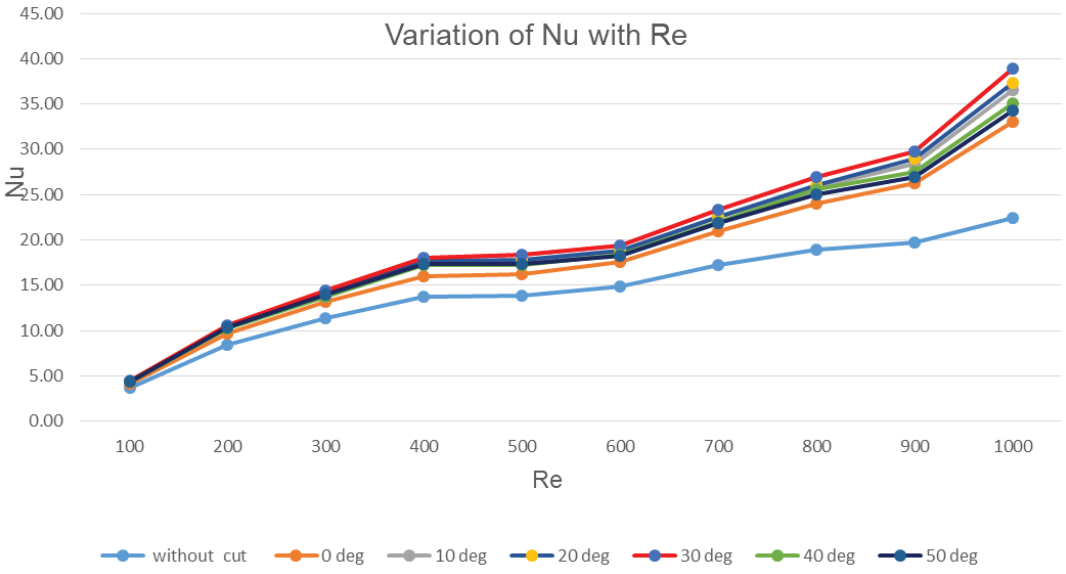


**Figure 30.** Variation of Nu for corresponding to change in Re for different geometries.

non-Newtonian behavior. Several fluid models have been proposed and studied to describe the dynamics of non-Newtonian fluids. One such model is the Ostwald-de-Waele power-law fluid, which finds extensive applications in engineering industries such as oil reservoir engineering, chemical engineering, and manufacturing processes. This model characterizes the flow behavior of certain non-Newtonian fluids, like polymer melts and glasses, which do not follow Newton's law of viscosity [24]. The integration of computers and electrical gadgets is important in today's technologically advanced world. Large-scale data management and monitoring are made easier by supercomputers and servers that are connected to several smaller computers. But these servers' closely spaced electrical parts, which produce a lot of heat, present problems. These heat-related problems are addressed externally by fans and air conditioners [25], and inside via heat-dissipating microchannel and flat plate heat sinks that use air or nanofluids [26]. Overheating still occurs in spite of these attempts, which reduces the dependability and longevity of electrical devices. The goal of innovations such as the combination of nanofluids [27] and cross-cut designs with wavy microchannels[28] is to reduce pressure drop, improve fluid flow mixing, and handle thermal issues in data-intensive server settings in order to prevent overheating.

Figure 30 depicts the results for Nusselt number as a function of Reynolds number. The Nusselt number rises as the Reynolds number rises [29]. This is due to the decrease in the thickness of the boundary layer in the heat sink as the velocity of the nanofluid increases. The cross

cut heat sink has a higher Nusselt number than the sans cut heat sink because to thermal boundary layer redevelopment [30]. Meanwhile, it is also noted that the initial Nusselt number increases as the angle of the oblique cut increases. Nanofluids are specifically designed colloidal suspensions of nanoparticles, usually less than 100 nm, in a base fluid. These fluids are potential for a variety of applications because they have distinct qualities from the basic fluid, such increased thermal conductivity. Typically, in Fluent, one creates a bespoke material by utilizing the mixture model to define the material characteristics of nanofluids. The effective properties of the nanofluid are a blend of the base fluid's and the nanoparticles' characteristics, and it is treated as a single continuous medium in this model. The volume fraction of nanoparticles in the fluid is then used to compute the nanofluid's characteristics. The concentration ratio, represented by the symbol φ, is the volume fraction of nanoparticles in the nanofluid. It shows the proportion of the nanofluid's overall volume to the volume of its nanoparticles. The material characteristics of the nanofluid are mostly determined by the concentration ratio; larger concentrations usually result in more notable changes in attributes. Numerous challenges in energy and geophysical industries, such as thermal insulation, geophysical flows, petroleum resources, and polymer processing, necessitate the analysis of free convective flow of non-Newtonian fluids in a porous medium. The majority of real fluids, including cosmetic products, grease, body fluids, and others exhibit non-Newtonian behavior. Studying non-Newtonian fluids in a porous matrix differs significantly from studying Newtonian fluids in porous media [31]. The associated complicated nondimensional governing equations were evaluated using a combination of local nonsimilarity and successive linearization techniques [32]. Heat and mass transfer vary significantly with the increase in nonlinear convection parameters, which depend on aiding and opposing flow situations. In both aiding and opposing flows, thermal dispersion enhances heat transfer, while the solutal dispersion parameter enhances mass transfer. This investigation is useful for understanding combustion mechanisms, aerosol technology, high-temperature polymeric mixtures, and solar collectors operated at moderate to very high temperatures [33].

## CONCLUSION

A details numerical (CFD) study has been performed to understand the impact of cross cut angle on heat transfer rate. Geometries of different cross cut angle 00, 100, 200, 300, 400 and 500 are simulated with heat flux 20000 w/mm$^2$. Also Experimental study has been carried to validate the results. Reynolds number is of range 100-1000 with hydraulic diameter 1 millimeter is used. The findings from present works are as follows

- Nusselt number increases with an increase of Reynolds number for all geometries because of decrease in thickness of boundary layer with increase in velocity.
- Geometry with cross cut gives more heat transfer rate than plane geometry due to combine effect of redevelopment of boundary layer and formation of secondary flow.
- It is found that geometry with 300 cross cut gives better heat transfer rate than that of other geometries (Experimentally 41 % more than without cut geometry).

In general heat transfer rate in microchannel is depending on angle of cross cut and input parameter like Reynolds Number. The study presented in this article provides valuable insights into the impact of cross-cut angles on heat transfer in microchannels. However, Investigation of the influence of surface modifications, such as roughness or coatings, on heat transfer enhancement in microchannels could provide further insights into enhancing heat transfer performance.

## AUTHORSHIP CONTRIBUTIONS

Authors equally contributed to this work.

## DATA AVAILABILITY STATEMENT

The authors confirm that the data that supports the findings of this study are available within the article. Raw data that support the finding of this study are available from the corresponding author, upon reasonable request.

## CONFLICT OF INTEREST

The author declared no potential conflicts of interest with respect to the research, authorship, and/or publication of this article.

## ETHICS

There are no ethical issues with the publication of this manuscript.

## REFERENCES

[1] Di Paolo Emilio M. Microelectronics: From fundamentals to applied design. Cham: Springer International Publishing; 2016. [CrossRef]

[2] Ma T, Du L, Sun N, Zeng M, Sundén B, Wang Q. Experimental and numerical study on heat transfer and pressure drop performance of Cross-Wavy primary surface channel. Energy Convers Manag 2016;125:80–90. [CrossRef]

[3] Rosengarten G, Cooper-White J, Metcalfe G. Experimental and analytical study of the effect of contact angle on liquid convective heat transfer in microchannels. Int J Heat Mass Transf 2006;49:4161–4170. [CrossRef]

[4] Dincer I, Genceli OF. Cooling process and heat transfer parameters of cylindrical products cooled both in water and in air. Int J Heat Mass Transf 1994;37:625–633. [CrossRef]
[5] Chu WX, Tsai MK, Jan SY, Huang HH, Wang CC. CFD analysis and experimental verification on a new type of air-cooled heat sink for reducing maximum junction temperature. Int J Heat Mass Transf 2020;148:119094. [CrossRef]
[6] Glazov A, Muratikov K. Laser thermal wave diagnostics of the thermal resistance of soldered and bonded joints in semiconductor structures. Sensors (Basel) 2023;23:3590. [CrossRef]
[7] Barron RF, Nellis GF. Cryogenic heat transfer. Boca Raton, Florida: CRC Press; 2017. [CrossRef]
[8] Balasubramanian K, Lee PS, Jin LW, Chou SK, Teo CJ, Gao S. Experimental investigations of flow boiling heat transfer and pressure drop in straight and expanding microchannels-a comparative study. Int J Therm Sci 2011;50:2413–2421. [CrossRef]
[9] Moharana MK, Singh PK, Khandekar S. Optimum Nusselt number for simultaneously developing internal flow under conjugate conditions in a square microchannel. 2012. Accessed on Dec 23, 2023. Available at: https://asmedigitalcollection.asme.org/heattransfer/article-abstract/134/7/071703/468117
[10] Khan MG, Fartaj A. A review on microchannel heat exchangers and potential applications. Int J Energy Res 2011;35:553–582. [CrossRef]
[11] Chen X, Li T, Zeng H, Hu Z, Fu B. Numerical and experimental investigation on micromixers with serpentine microchannels. Int J Heat Mass Transf 2016;98:131–140. [CrossRef]
[12] Aglawe KR, Yadav RK, Thool SB. Fabrication, experimentation and numerical simulation of microchannel heat sink for enhancing thermal performance of electronic devices. Int J Interact Des Manuf 2023;18:1–16. [CrossRef]
[13] Alfaryjat AA, Mohammed HA, Adam NM, Ariffin MKA, Najafabadi MI. Influence of geometrical parameters of hexagonal, circular, and rhombus microchannel heat sinks on the thermohydraulic characteristics. Int Commun Heat Mass Transf 2014;52:121–131. [CrossRef]
[14] Javaid Afzal M, Tayyaba S, Khan MI. A review on microchannel fabrication methods and applications in large-scale and prospective industries. Evergreen 2022;9:764. [CrossRef]
[15] Rui Z, Zhao F, Sun H, Sun L, Peng H. Experimental research on flow boiling thermal-hydraulic characteristics in novel microchannels. Exp Therm Fluid Sci 2023;140:110755. [CrossRef]
[16] Geyer PE, Fletcher DF, Haynes BS. Laminar flow and heat transfer in a periodic trapezoidal channel with semi-circular cross-section. Int J Heat Mass Transf 2007;50:3471–3480. [CrossRef]
[17] Kurtulmuş N, Zontul H, Sahin B. Heat transfer and flow characteristics in a sinusoidally curved converging-diverging channel. Int J Therm Sci 2020;148:106163. [CrossRef]
[18] Yotsukura N, Sayre WW. Transverse mixing in natural channels. Water Resour Res 1976;12:695–704. [CrossRef]
[19] Naveen P, RamReddy C, Srinivasacharya D. Nonlinear convective flow of power-law fluid over an inclined plate with double dispersion effects and convective thermal boundary condition. In: Ray SS, Jafari H, Sekhar TR, Kayal S, editors. Applied analysis, computation and mathematical modelling in engineering. Singapore: Springer Nature Singapore; 2022. p. 109–127. [CrossRef]
[20] Law M, Lee PS, Balasubramanian K. Experimental investigation of flow boiling heat transfer in novel oblique-finned microchannels. Int J Heat Mass Transf 2014;76:419–431. [CrossRef]
[21] Naveen P, RamReddy C. Quadratic convection in a power-law fluid with activation energy and suction/injection effects. Int J Ambient Energy 2023;44:822–834. [CrossRef]
[22] RamReddy C, Naveen P. Analysis of activation energy in quadratic convective flow of a micropolar fluid with chemical reaction and suction/injection effects. Multidiscip Model Mater Struct 2020;16:169–190. [CrossRef]
[23] RamReddy C, Naveen P. Analysis of activation energy and thermal radiation on convective flow of a power-law fluid under convective heating and chemical reaction. Heat Transf Asian Res 2019;48:2122–2154. [CrossRef]
[24] RamReddy C, Naveen P, Srinivasacharya D. Nonlinear convective flow of non-Newtonian fluid over an inclined plate with convective surface condition: A Darcy-Forchheimer model. Int J Appl Comput Math 2018;4:51. [CrossRef]
[25] Gupta S, Carmichael C, Simpson C, Clarke MJ, Allen C, Gao Y, et al. Electric fans for reducing adverse health impacts in heatwaves. Cochrane Database Syst Rev. 2012. [Epub ahead of print]. doi: 10.1002/14651858.CD009888.pub2 [CrossRef]
[26] Gunnasegaran P, Shuaib NH, Mohammed HA, Jalal MA, Sandhita E. Heat transfer enhancement in microchannel heat sink using nanofluids. Fluid Dyn Comput Model Appl 2012;287–326. [CrossRef]
[27] Rashidi S, Eskandarian M, Mahian O, Poncet S. Combination of nanofluid and inserts for heat transfer enhancement: Gaps and challenges. J Therm Anal Calorim 2019;135:437–460. [CrossRef]
[28] Zhou J, Hatami M, Song D, Jing D. Design of microchannel heat sink with wavy channel and its time-efficient optimization with combined RSM and FVM methods. Int J Heat Mass Transf 2016;103:715–724. [CrossRef]

[29] Hadjiconstantinou NG, Simek O. Constant-wall-temperature Nusselt number in micro and nano-channels. J Heat Transf 2002;124:356–364. [CrossRef]

[30] Zhou F, Catton I. Numerical evaluation of flow and heat transfer in plate-pin fin heat sinks with various pin cross-sections. Numer Heat Transf Part A Appl 2011;60:107–128. [CrossRef]

[31] RamReddy C, Naveen P, Srinivasacharya D. Influence of non-linear Boussinesq approximation on natural convective flow of a power-law fluid along an inclined plate under convective thermal boundary condition. Nonlinear Eng 2019;8:94–106. [CrossRef]

[32] Srinivasacharya D, RamReddy C, Naveen P. Effects of nonlinear Boussinesq approximation and double dispersion on a micropolar fluid flow under convective thermal condition. Heat Transf Asian Res 2019;48:414–434. [CrossRef]

[33] Srinivasacharya D, RamReddy C, Naveen P. Double dispersion effect on nonlinear convective flow over an inclined plate in a micropolar fluid saturated non-Darcy porous medium. Eng Sci Technol Int J 2018;21:984–995. [CrossRef]